Estimation of Knee Joint Impedance During Walking and its Implications for Robotic Control and Beyond

by

Yves F. Nazon II

A dissertation submitted in partial fulfillment
of the requirements for the degree of
Doctor of Philosophy
(Mechanical Engineering)
in the University of Michigan
2024

Doctoral Committee:

Associate Professor Elliott J Rouse, Chair
Professor Brent Gillespie
Associate Professor Robert Gregg
Associate Professor Leia Stirling

*"Once you know your **why**, you'll know your **way**"* – Deborah Nazon

Yves Nazon II

nazon@umich.edu

ORCID iD: 0000-0002-4798-7223

I dedicate this to all the PhD students who's path deviated from what was expected and you persevered anyways

ACKNOWLEDGEMENTS

I want to start by giving all glory to God. Jeremiah 29:11 says "For I know the plans I have for you," declares the Lord, "plans to prosper you and not to harm you, plans to give you hope and a future.". When I started this PhD journey I didn't know what those plans were and at multiple times I struggled with why I was completing this degree. Whether it was struggling through changing schools, getting on and off academic probation twice, or a truly INNUMERABLE amount of research failures, I had many points when I questioned those plans. However, I want to thank God for staying true to the promise that you would never leave me, nor forsake me. That allowed me to stay true to my promise to trust in you, and ultimately, lead to me finishing this degree and graduating.

Next, I want to thank my parents Deborah Nazon and Yves Nazon. I cant even imagine where I would be without the two of you. My biggest cheerleaders, whether it be loudly to the world or in your own quiet way, the love you've shown me my entire life has been and is one of the largest factors in my success. Dad, you were the first engineer I ever met, even though I didn't know it, and you are one of the most amazing ones I know. You can fix anything. I feel so fortunate that some your mechanical prowess passed on to me, and I hope to be as resourceful and mechanically adept as you are one day. For my Mom aka mommy aka mother of dang, I love you so much. Thank you for being your own trinity in one, Mom mom, PhD mom, and BFF mom. Your constant advice has kept me going and has guided me during multiple

times where I didn't know what to do. Thank you for laying the path before me as the first Dr Nazon in our household. I love the both of you so much and I dedicate part of this PhD to you.

I want to give massive thanks to my committee. Some people don't have, or choose to not have, their committee members be an active part of their PhD process. However, I was fortunate to have you all be an active and important part of my process. To Brent, I want to say thank you for your incredibly useful insights. Whether is was giving feedback on goniometer placement during the early parts of my experiments or giving a useful different take on impedance, your feedback has significantly helped craft this work and I am thankful to you for that. To Leia, you have provided so much warmth to this, at times, cold and isolating process. The technical insights of you and your students has been incredibly helpful with my experimental design. However, what resonates with me the most is your warmth and the care you have shown for me as a person. You give a warm beating heart to the cold machines we work with, and it is that warmth that I have found to be invaluable when things were tough. To Bobby, my unofficial second advisor, you have been incredibly gracious with lending your resources to aid me in the completion of my PhD work. You and your students have given me countless pieces of advice on how to work with MBLUE. Without you all, I do not finish this project. I want to truly thank you for your guidance and giving spirit. Lastly, but certainly not least, I want to say thank you to my advisor Elliott Rouse. Elliott, words cannot express how grateful I am that you were my advisor. Your incredible ability as an engineer is something I have always admired and have hoped would rub off on me. Two schools and eight years later, I can confidently say that some of your amazing engineering ability has indeed rubbed off on me and I am a much better engineer and person for it. I want to thank you for your patience with me as I have grown into the engineer and scientist I am today. The process of growing together has not always been easy, but I am proud to see how

far we have both come.

To the Neurobionics lab, past and present, and the NeuroLoco lab I want to thank you for the support, encouragement, knowledge transfer, and good times. I especially want to thank Alejandro Azocar, Tyler Clites, Nikko Van Crey, Kim Ingraham, Leo Medrano, Kevin Best, and Riley Pieper for being phenomenal friends, confidants, and colleagues over the years. I have had the best work place colleagues anyone could ever ask for. Any place I work after this will have a tough act to follow.

To my family, I want to thank you for always lifting my spirits. There has never been a time when I have spent time with you and have not left happier than I arrived. To the Nazon's, we OBJECTIVELY have the best family ever and I am constantly amazed at how our diverse lives and physical makeups are unified by how wonderful we all are as people. Yam wars is the greatest thanksgiving tradition of all time, and being able to beat you all in dominoes, year in and year out, is a pleasure I don't take for granted. The way my soul is replenished every time I spend time with y'all is one of my greatest joys and I am so thankful for you. To the Ingram's, I dedicate my grit, savvy, and cooking ability to you. Whenever I leave Maryland or Philly, I always feel like I just received the best warm hug. Being able to see the family grow has been beautiful and I look forward to being able to spend more time with you and the little ones in the future.

Lastly I want to thank my friends. There are too many of you to name all of you but thank you for always enveloping me in love. To my NY people: the Macedonia crew, the S6, the Hurley's, Burgoses, Zuber's and so many more, thank you for giving me my start. For always having a warm hug or warmer meal for me whenever I am home. For believing in my ability from the beginning and always encouraging me. To my Northwestern people, while it was briefer than I wanted it to be, my time in Chicago was a movie. Going through the trenches with y'all in the early parts of

grad school and decompressing in the city are some of my fondest memories. To see our friendships not only maintain but blossom over time has been super rewarding and fills me with glee. To Jann, Self, Chamomile, Liane, Zay, Sal, Nisan, Mecca, Lydia, Marc, Andrea, Mikhail, Matt, Abby, and Karen (KJAMS) y'all are really and truly wonderful. I can't imagine what my time in Chicago would have looked like without y'all. To my Michigan folk, what can I say that isn't symbolized in the way I hit the hustle or cheer out "Go Blue" at any Michigan sporting event. You all have been my main support system throughout this PhD. Taking me to football games, introducing me to amapiano, or sharing food downtown, you all have been the rock upon which my time was built. I want to give an extra big shoutout to Wilka Carvalho, Dominic Bednar, Donald Richardson, Vani Ravichandran, Kori McDonald, Haley Sparks, Channing Mathews, Ivan and Evvy Tibavinski, Jose Montes, Bella Okiye, Taylor Bramlett, Ayza Croskey, Courtney Smith, and Kweku Abimbola for the pivotal role you played in my time here. And finally, to my UMBC people, wow ... I love you. They say friends are the family you choose and I could not think of a better way to describe how I feel about all of you. To Mr. Lamont Toliver, you are the greatest man I have ever met, I know I've made you proud and I will keep chasing the standard of greatness that you have set and shown through your actions. To Dr. Hrabowski and the Meyerhoff scholars program, thank you for allowing me to be a part of the next wave of leaders and scholars in the greatest pre-PhD, development program in the country. Thank you for allowing me to find my tribe. Before UMBC, I never imagined it would be possible for me to be around so many smart, fun, witty, intelligent, hilarious black and brown people that I had so much in common with in one place. Thank you for giving me the opportunity to travel the country and hold the banner for the Meyerhoff scholars program as one of its representatives. Thank you for giving me the opportunity to go to college essentially for free. You all gave me my start and I will never forget that nor be able to thank you enough. To my

23's, I could have never imagined that when we met at 17 and 18 years of age that I would be meeting the core of my closest friends. I couldn't have dreamed of the moments we would share together: traveling across the world together, being at each other's weddings, supporting one another through deaths, the birth of children, and so much more. It has only been through leaving UMBC that I realized how rare it is to have friends that are as amazing, reliable, and incredible as you all. Most people are lucky to have 1 or 2 people like this in their life; I have at least 10 of them in my cohort alone. It truly boggles my mind how blessed I am to have you all in my life, and there are not enough words in the world or prayers that I could pray, that would appropriately convey how I feel about you all and how much I love you. To Quentin (Que), Iffy (EEEE-FAYY-LUUUU), John (Johnny R), Sam (Juice Man Sam), Pelumi (Lu), Sagar (Sags), Larry (LarBear), Em (the scientist formally known as Michael), Juliette (Hooles), Jichele (Chele), and Saiah (Sai-Sai aka Shanel) while I write thank you here, just know that it isn't anywhere close to enough to say how much I love you and how thankful I am that you are in my life.

TABLE OF CONTENTS

LIST OF FIGURES

Figure

LIST OF TABLES

Table

LIST OF NOMENCLATURES

ADL Activities of Daily Life

IRF Impulse Response Function

LTI Linear Time Invariant

LTV Linear Time Variant

FGWN Filtered Gaussian White Noise

QDD Quasi-Direct Drive

NPC No Perturbation Condition

APC Applied Perturbation Condition

E-NPC Exoskeleton No Perturbation Condition

E-APC Exoskeleton Applied Perturbation Condition

GRF Ground Reaction Force

MBLUE Modular Backdrivable Lower-limb Unloading Exoskeleton

NWC Non-Exoskeleton Walking Condition

ENP Exoskeleton Walking With No Perturbations

EWP Exoskeleton Walking With Perturbations

ICO Initial Contact

LRE Loading Response

MST Mid-Stance

TST Terminal Stance

PSW Pre-Swing

ISW Initial Swing

MSW Mid-Swing

TSW Terminal Swing

SPM Statistical Parametric Mapping

ABSTRACT

The mechanical impedance of the human lower-limb joints during locomotion encodes our understanding of how the human feedback system stabilizes the body and is a key component of several strategies for translating this behavior to robots, to powered prosthetic limbs, and to people empowered by exoskeletons. Knowledge of how this property varies in lower limb joint is sparse, with the amount of information available decreasing as you move up the kinematic chain from the ankle to the hip. This work looks to broaden the knowledge base of how knee impedance is modulated, particularly during the process of ambulation. This work first provides an overview of the lower limb joint impedance literature, and from this overview, produces three aims to address current gaps in the knowledge base. The first aim validates the use of methods for impedance estimation. The second aim characterizes a device that can be used to estimate impedance, and utilizes that device to estimate knee impedance in a pilot study. The third aim produces estimates of knee impedance during walking for a group of abled bodied participants. Finally, this work discusses the implications of the work produced on the fields of human system identification, wearable robotics, and rehabilitation, concluding with recommendations for future work.

CHAPTER I

Introduction

1.1 Motivation

Careful regulation of lower limb joint mechanics is a necessity for the completion of activities of daily life (ADL's). These mechanics—collectively known as *joint mechanical impedance*—govern the body's instantaneous response to disturbances and regulate energy storage and exchange during movement [1, 2, 3]. Previous studies have shown the human ability to regulate joint impedance, both consciously and subconsciously, to adapt to unexpected changes during dynamic tasks [4, 5, 6]. The characterization of lower limb joint impedance has significant implications for studying and improving locomotion, including insights into human motor control, treatment of neuromotor pathologies, and the development and control of biomimetic assistive technologies [7].

1.2 Background

Knowledge of joint mechanical impedance has many application areas spanning basic science, robotics, and rehabilitation. Mechanical impedance governs the exchange of energy between joints in the body which allows us to complete ADL's like walking, running, and jumping [2]. There even exists the theory that the body uses the impedance to control our central nervous system [4]. The impedance parameters of

the body also govern how we respond to disturbances while we're doing those ADL's. Examples include our ability to respond to slips, trips, and falls when the environment does not behave like we expect [8]. Impedance also is useful in the development and control of assistive devices for people who's ability to complete ADL's has been impaired or lost. A common strategy in the control of prosthetics and orthotics is using biological, or biologically motivated, impedance values to control these devices [7, 9, 10, 11]. Impedance control is a valuable tool for these devices because it combines the benefits of two other common control strategies, torque and position control. It also provides the user with the ability to adapt to environments that may change rapidly or unexpectedly. Knowledge of how the body changes its impedance is also used as a design requirement for prosthetic devices [12, 13, 14]. Knowledge of impedance values translates to output torque and power requirements for prosthetic actuators. This is a major guiding factor the design of wearable devices that must to balance factors such as weight, power density, form factor, and performance.

Having a quantitative framework to describe joint mechanical impedance is crucial for interpretation of the results from impedance experiments. Joint mechanical impedance is defined as the relationship between an input position, or one of its derivatives, and an output torque [15]. The inverse of a linear mechanical impedance is admittance, where torque is the input and position, or one of its derivatives, is the output. The measurement of human joint mechanical impedance mandates three acts must occur: the joint in question must be perturbed, the torque about the perturbed joint must be measured, and the position displacement, or one of its derivatives, of the joint during the perturbation must be measured. While mathematically, estimates of impedance and admittance are inverse rendering the input of torque or position inconsequential, it is important to note that functionally, the noise on the input signal will effect the estimates of impedance. Restated differently, this means that whether the input is position or torque will have an effect on the estimates. Position inputs

are better for obtaining estimates at high frequencies while torque inputs provide better system estimates at low frequencies. There are multiple mechanisms that effect joint impedance, of which some of the most notable are: the inertial dynamics of the limb attached to the joint of interest, the external torque applied to the joint, the viscoelastic properties of the joint, the dynamics of the muscles that span the joint, the muscular reflexes, and the bilateral use of the muscles that span the joint of interest [1]. Modeling all of these components can be challenging, resulting in multiple approaches to mathematically describe this behavior.

When mathematically describing the impedance of a joint, the most thorough way to model a system is to use a nonparametric model. When using nonlinear nonparametric models for impedance estimation, a common assumption is that the system being identified is linear and displays time invariant behavior. Under this assumption multiple models have been formed. [1, 16]. Linear nonparametric models can be crafted in the frequency or time domains. Many frequency response nonparametric models take the form of 1.1 where $\tau(j\omega)$ is the Fourier transform of torque, $H(j\omega)$ is the impedance frequency response, and $\theta(j\omega)$ is the Fourier transform of displacement. A frequency response estimate of the impedance transfer function can be obtained by looking at the relationship of the auto spectral density of the displacement signal, $\Phi_{\theta\theta}$, and the cross spectral density of the torque and displacement signals, $\Phi_{\tau\theta}$, (1.2).

$$\tau(j\omega) = H(j\omega)\theta(j\omega) \tag{1.1}$$

$$\hat{H}(j\omega) = \frac{\Phi_{\tau\theta}}{\Phi_{\theta\theta}} \tag{1.2}$$

In the time domain, the nonparametic model of impedance is obtained from the

impulse response function or IRF. An IRF conveys how a dynamic system responds to an input impulse. The impedance IRF demonstrates how a system, $h(\tau)$, responds to an input position, $\theta(t-\tau)$, and yields an output torque, $T(t)$ (1.3). To produce an estimate of the impedance transfer function in the time domain, $\hat{h}(\tau)$, one uses the Weiner-Hopf relationship which relates the autocorrelation of the displacement signal, $r_{\theta\theta}$, and the cross correlations of the torque and displacement signals $r_{T\theta}$ (1.4) [17, 16].

$$T(t) = \int_{-\infty}^{\infty} h(\tau)\theta(t-\tau)d\tau \tag{1.3}$$

$$r_{T\theta}(\tau) = \int_{-\infty}^{\infty} \hat{h}(\tau)r_{\theta\theta}(t-\tau)d\tau \tag{1.4}$$

While nonparametric impedance models have the benefit of more accurately representing system behavior, less complicated parametric models can exploit their simplicity for superior real-time implementation on robotic systems. Another benefit of parametric models is that they can be contrived in such a way that the model has physical relevance. An example of this is the commonly used parametric model for human joint impedance, a second order dynamical system with an input position, θ, output torque, $T(t)$, stiffness constant, K, damping value, B, and inertia, I (1.5). This model of impedance has been shown to accurately describe greater than 97% of the variance of an impedance IRF for a human ankle joint [1].

$$T(t) = K\theta + B\dot{\theta} + I\ddot{\theta} \tag{1.5}$$

The circumstances under which impedance is measurable can be distilled down to

two options: static and dynamic conditions. Joint impedance has been characterized under static conditions far more often than dynamic conditions. In the lower limbs, static studies have been conducted at the hip, knee, and ankle. At the hip, some static studies have been conducted [18, 11]. At the knee, static impedance characterization work started in the 70's and persisted to the late 90's [19, 20, 21, 22]. The ankle has been the most characterized lower limb joint with multiple studies being performed by numerous researchers [1, 23, 24, 25, 26, 27]. Dynamic joint impedance studies are typically more involved, and therefore have been explored far less. There are few recorded dynamic impedance studies for the hip and knee [28, 29, 30, 16]. Similarly to the static case, the ankle is the most studied joint in the case of dynamic impedance measurements. Of these dynamic ankle studies, one subset of experiments worth noting are those occurring during locomotion. Locomotion tasks are commonly explored because of the breadth of ADL's that involve locomotion.

How dynamic impedance changes during locomotive tasks has been studied at all lower limb joints, but with varying degrees of depth. A few studies have captured snapshots of how impedance varies at the hip and knee [30, 16], however the only lower limb joint where impedance has been fully characterized is the ankle [31, 32]. Knowledge of how impedance varies dynamically is important and should not be seen as an academic exercise. Ludvig *et al.* have shown that at the knee, impedance measured during dynamic motion is lower than impedance measured during static positions [29]. This result reinforces the need to characterize joint impedance under dynamic conditions; serving as a reminder to the field that there is still much to learn about lower limb impedance and, particularly at the knee and hip, creating many opportunities for research.

One of these open research questions is how does one capture and record the information necessary to estimate impedance during active tasks. Literature shows the

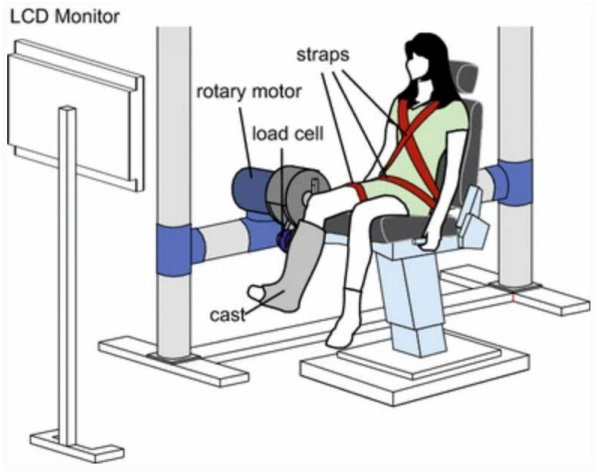

Figure 1.1: *Cartoon of a dynomometer setup taken from Ludvig et al.*

current devices capable of meeting these requirements can take many forms. Some of the first devices used to identify dynamic impedance were seated dynomometer setups [29, 33]. In these configurations, users are attached to the dynomometer through an attachment that permits the joint of interest to rotate freely. One of the drawbacks of this type of system, is that the subjects are not able to do active tasks, like walking, because they are attached to the dynomometer which cannot move.

A system that overcomes the motion constraint imposed by the dynomometer and permits dynamic impedance information recording is the recessed force platform [34, 35, 36, 37]. Recessed force platforms are commonly operated in concert with a displacement measurement system, like motion capture or an electrogoniometer, to gather impedance information. Fortunately, these systems do not constrain the user's motion like dynomometer systems do. Unfortunately, a draw back of these systems is that the foot must be in contact with the platform to apply a perturbation. This means for portions of activities where the user is not on the ground, like jumping for example, these device cannot be used. These devices also require the user to walk on them in specific ways which can lead to abnormal motion.

A way to overcome the foot contact constraint of the recessed force platform is to use

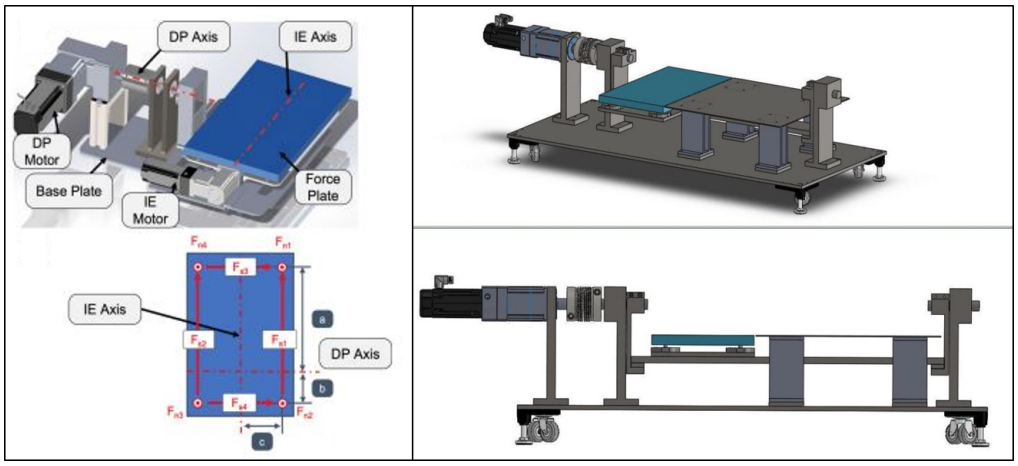

Figure 1.2: *Recessed force platforms used in perturbation experiments. Left shows a device used by Russell et al. of a dual recessed platform used for perturbation studies conducted during walking and running. Right shows a 3D model of the Perturberator robot recessed force platform taken from Elliott Rouse's work*

a pulling system [38, 16]. These systems use off board cables and motors to apply a linear force to a user. A benefit to these systems is that they can apply perturbations to users regardless of if the joint of interest is grounded or not. Regretfully, these systems generally require a model to convert the linear force to a torque about the joint. During this process there can be unmodeled system dynamics, like cable slack for example, which make the force experienced by the user different than expected, affecting results.

A versatile device that can bypass many of issues is the exoskeleton. Exoskeletons can provide the benefit of minimally effecting human motion while allowing perturbations to be directly applied to the joint of interest, avoiding the need for a translational model. Previous studies have used exoskeletons to estimate joint impedance during various points in the gait cycle for the knee and ankle [25, 39, 30]. While these studies exist, no one has yet to quantify, if and how, impedance varies throughout the entire gait cycle at the knee.

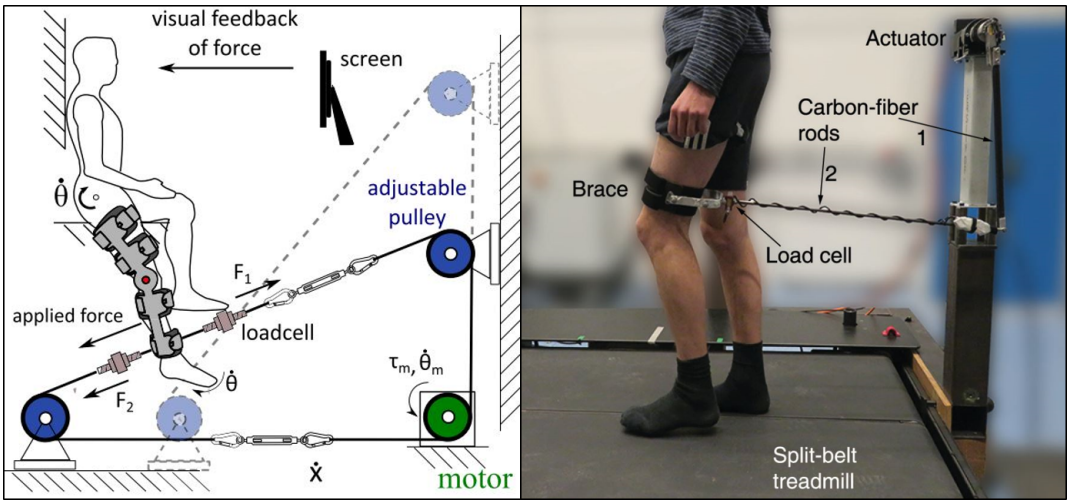

Figure 1.3: *Pulling system perturbation devices. Left shows Huang et al. using pulling system for perturbing the hip. Right shows Kooji et al. pulling system for combined hip and knee perturbations*

1.3 Specific Aims

This work addresses the gap in knowledge of, if and how, mechanical impedance varies at the knee joint during locomotion through the original usage of existing methods and technologies. This work utilizes an existing method for impedance estimation and demonstrates an improvement upon the method's previously reported error measurements. This work also applies this method to exoskeleton systems for the first time. This work provides the first reported knee impedance values during the stance phase of walking. It also provides new insights on how knee impedance varies during the swing phase of walking by providing data at points that have never been recorded before. Finally, this thesis provides the first account of using a modular, back-drivable, exoskeleton for human system identification by using this device in a completely novel configuration. This work accomplishes these feats through the completion of three targeted project aims.

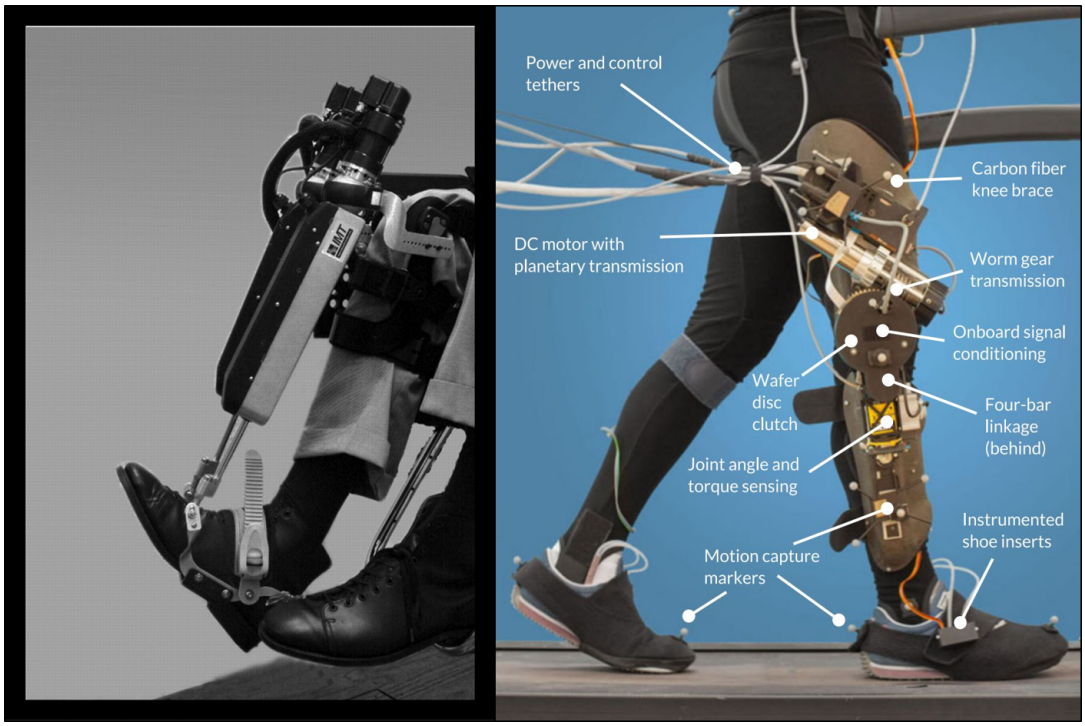

Figure 1.4: *Exoskeleton systems used for perturbation application and impedance estimation. Left is the MIT Anklebot used by Lee and Hogan. Right is the ETH Knee Perturberator used by Tucker et al.*

1.3.1 Aim 1: Validate Methods For Estimating Joint Mechanical Impedance Using An Exoskeleton

Aim 1 presents the validation of methods for estimating knee joint mechanical impedance during locomotion using a torque-controllable knee exoskeleton. In this aim, I utilize an exoskeleton to apply torque perturbations to different spring mass systems and measure the resultant position displacements. The displacement and torque information, measured by the exoskeleton, is used to estimate the stiffness and inertia value of the spring mass systems. This aim provides the foundation of the methods that will be later used to estimate the joint mechanical impedance of the knee.

1.3.2 Aim 2: Characterize The System Identification Abilities Of A Wearable Robotic Device For Human System Identification

Aim 2 is the characterization of a quasi-direct drive actuator. In this aim, I first create a model to estimate the torque output of the actuator using state information from the actuator. Then I use this torque model, as well as encoder information from the actuator, to estimate the stiffness of a mechanical system under static and dynamic conditions. After characterizing the stiffness estimating capabilities of the actuator, I incorporate the device in to a knee exoskeleton module, conduct a perturbation experiment on two individuals, and estimate the mechanical impedance of the participants from the experimental data. This aim produces a device that is capable of estimating knee joint impedance.

1.3.3 Aim 3: Estimate Human Knee Joint Mechanical Impedance During Walking

Aim 3 is the estimation of knee impedance using an exoskeleton as a perturbation device. I leverage the estimation techniques used in aim 1 and the device characterized in aim 2, to estimate the knee joint mechanical impedance of 10 able-bodied subjects during treadmill walking. Knee impedance is estimated at multiple points of the subjects gait cycle, encompassing both the stance and swing phases of gait. The work in this aim, presents the first experimentally obtained estimates of knee impedance during the stance phase of gait. This aim also produces impedance estimates for previously unidentified portions of the swing phase of gait.

To inform the reader how these scientific strides were made, this dissertation highlights the validation of the methods used for impedance estimation in chapter two. Chapter three addresses aim 2, by demonstrating the work done to characterize an actuator's system identification abilities. In chapter four, this work then applies chapter two's

estimation methods to human subjects, using the device presented in chapter three, yielding knee impedance estimates during six phases of gait. This work is concluded in chapter five by summarizing the findings of chapters two, three, and four; pontificating about how these results can impact future research for academic, commercial, and clinical endeavors.

CHAPTER II

Validation of Methods for Estimation of Knee Joint Mechanical Impedance During Locomotion Using a Torque-Controllable Knee Exoskeleton

2.1 Introduction

Careful regulation of dynamic properties of the knee is integral for successful human locomotion. Knowledge of how these dynamic properties are modulated is essential to understanding how humans achieve stable gait as muscles spanning this joint provide critical support to the body and decelerate the limb during stance, deliver power to accelerate the trunk [40], and absorb energy at the end of the swing [41]. One of these properties, known as joint impedance, governs the body's instantaneous response to disturbances and regulates energy exchange at joints during movement [1]. Studies have demonstrated that humans regulate joint impedance subconsciously to adapt to unexpected changes during dynamic tasks [4, 5]. A thorough characterization of knee impedance has significant implications for studying and improving locomotion. Examples of these implications are insights into human motor control, treatment of neuromotor pathologies, and development of biomimetic assistive devices.

While knee impedance has been extensively studied under certain conditions, a holis-

tic understanding of this property still evades the field. The impedance of the knee has been characterized during postural tasks and noted to vary with joint angle and muscle activation level [1, 42]. Several studies have demonstrated that joint impedance during dynamic tasks is different from postural ones [43, 44, 45]. While some studies have generated model-based estimates of knee impedance during movement [46, 47, 48] or characterized the torque-angle relationship of the knee during gait [49] (which is different from the stiffness of the knee [50]), no one has validated these results experimentally.

Measurement of joint impedance requires the application of an external perturbation. There are two perturbation paradigms available to this end: applying a torque perturbation and measuring the resulting change in position, or perturbing the joint position and observing the developed torque response [1]. There exist a number of exoskeletons designed to perturb the knee during locomotion [51, 52, 53, 54]. These exoskeletons employ a range of perturbation paradigms including flexion/extension locking [51], knee flexion torque assistance [52], and angular positional perturbations [53, 54]. However, these exoskeletons cannot provide perturbations bidirectionally, with certain exceptions such as Tucker et. al. Further, none of these devices have been used to quantify knee impedance in static or dynamic conditions.

Estimation of joint impedance from experimental data is typically attained using linear techniques. Linear techniques commonly describe joint impedance in terms of an nonparametric impulse response function or a parameterized second-order system consisting of stiffness, damping, and inertia [1]. The parametric version of impedance can be obtained using linear time invariant (LTI) or linear time variant (LTV) methods. Previous work used a parametric approach to characterize the dynamic impedance of the ankle over the entire gait cycle, employing both LTI and LTV methods [2, 39, 32]. [39] utilized a wearable ankle device to provide controlled torque perturbations to the

ankle directly during the swing phase and extracted impedance parameters using LTV methods. [2, 32] took a different approach, leveraging an instrumented walkway to apply angular perturbations to the ankle indirectly during the stance phase and obtaining impedance parameters through LTI data analysis.

The contribution of this paper is validating the novel combination of experimental and analytical methods for estimating mechanical impedance with a torque-controllable knee exoskeleton. We propose using a torque perturbation paradigm with an untethered, wearable knee exoskeleton that can apply torques bidirectionally. We will use LTI methods to estimate the mechanical impedance of known mass spring systems. We postulate the benefits of this approach are multi-faceted. LTI methods are simpler to perform than LTV, an untethered and wearable device allows data collection during all portions of the gait cycle across multiple types of terrain, and bidirectional perturbations permit exploration impedance during flexion and extension. We will demonstrate the efficacy of our methods and device through characterization of the exoskeleton's torque bandwidth and intrinsic impedance properties and validation of the system identification capabilities of the device through use of the proposed perturbation paradigm. Implementation these methods with this device and analysis of the results will provide a framework for future methods towards the goal of characterizing the impedance of the human knee during locomotion.

2.2 Methods

2.2.1 Torque-Controllable Exoskeleton

We propose the use of a torque-controllable exoskeleton developed by Shepherd et al.; a full description of the device is found in [55].Briefly, a brushless dc motor (EC30, Maxon Motor, Sachseln, Switzerland) drives a 2.5 mm lead ball screw (Thomson Industries, Inc., Radford VA, USA) after a 2:1 belt drive (2.1). A two-force member

connects the ball nut to a cantilever fiberglass beam (Gordon Composites, Montrose, CO, USA). This fiberglass beam functions as a series elastic element between the transmission and the output, with a translational stiffness of 274 N/mm to a perpendicular load. Two submicron resolution optical encoders (ATOM; Renishaw, Wotton-under-Edge, Gloucestershire, UK) placed before and after the spring in the drive train measure the angular deflection of the spring. This angular deflection is used to generate an estimate of measured torque (2.2). Torque control of the exoskeleton is implemented on a python-based Raspberry Pi microcontroller (model: Raspberry Pi 3 Model B, Raspberry Pi Foundation, Cambridge, UK).

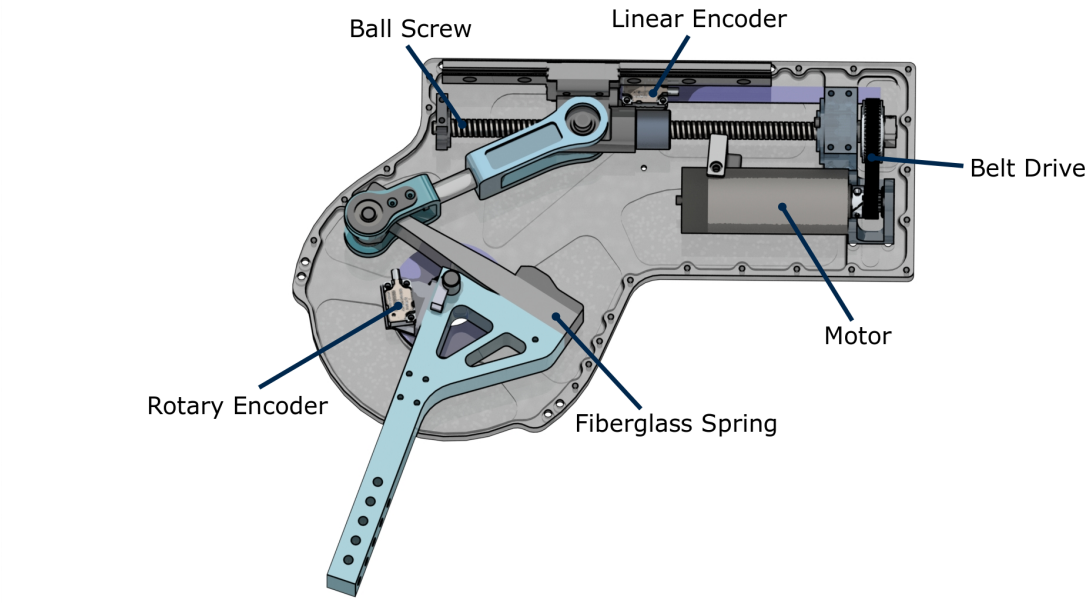

Figure 2.1: *Diagram of the Neurobionics torque-controllable exoskeleton. The fiberglass spring serves as the series elastic element in the actuator, connecting the transmission to the output shaft.*

2.2.2 Characterization of Exoskeleton Bandwidth and Intrinsic Impedance

We characterized the system's bandwidth and intrinsic impedance to validate the use of the exoskeleton as an impedance measurement tool. To determine system

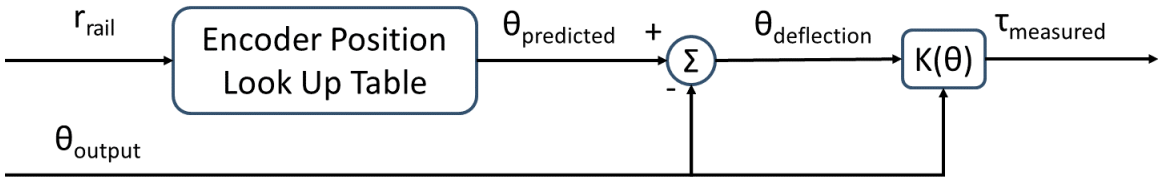

Figure 2.2: *Block diagram of exoskeleton torque calculation. Deflection of the fiberglass spring is calculated as the difference between the position estimated by the linear encoder and the position measured by the rotary encoder. This deflection is multiplied by the position-dependent stiffness of the fiberglass spring to provide an estimate of the torque applied by the exoskeleton.*

bandwidth, two Gaussian white noise signals with amplitudes of 20 and 40 Nm, low-pass filtered using a third-order Butterworth filter with a cut-off frequency of 40Hz, were provided to the exoskeleton. We measured the system's output torque (τ) and applied the spa function in MATLAB (MathWorks, Natick, Massachusetts) to determine the system's bandwidth. To characterize the intrinsic impedance of the device, we applied a time domain-based parametric system identification technique. A reference position trajectory in the form of a Gaussian white noise signal was low-pass filtered using a third-order Butterworth filter with a cut-off frequency of 20 Hz. The filtered signal was provided to the device for three 30-second trials, during which actuator output position (θ(t)) and measured torque (τ) were collected at a sample rate of 1 kHz. Following data collection, a least-squares regression implemented in MATLAB was used to resolve stiffness (K), damping (B), and inertia (J) estimates from output position and measured torque using the relation in 2.1.

$$\tau = J\ddot{\theta}(t) + B\dot{\theta}(t) + K\theta(t) \tag{2.1}$$

Following estimation of the parameters in 2.1, a second-order impedance model was generated to compare the frequency response of the measurements to that of the model.

2.2.3 Dynamic Estimation of Mechanical Impedance

The exoskeleton's system identification capabilities and the proposed methodology for estimating dynamic mechanical impedance were validated by perturbing a set of known mass-spring systems. We matched two inertias ($I_1 = 0.0364 \pm 4.97\text{x}10^{-5}$ kgm^2, $I_2 = 0.0700 \pm 2.04\text{x}10^{-4}$ kgm^2) to two springs ($k_1 = 168 \pm 14.3$ Nm/rad, $k_2 = 273 \pm 13.9$ Nm/rad) to test four spring-mass combinations. The mass-spring combinations tested are referred to as cases 1-4 hereafter, where case 1 is k_1 matched with the I_1, case 2 is k_2 matched with I_1, case 3 is k_1 matched with I_2, and case 4 is k_2 matched with I_2. During benchtop tests, the tested inertia was rigidly attached to the output shaft and the tested spring was suspended between the output shaft and a fixed stand 2.4). We chose inertia values that correspond to one half (I_1) and one (I_2) times the inertia of the human shank and foot [56]. We chose spring stiffness values that span the range of human knee stiffness values in literature [42].

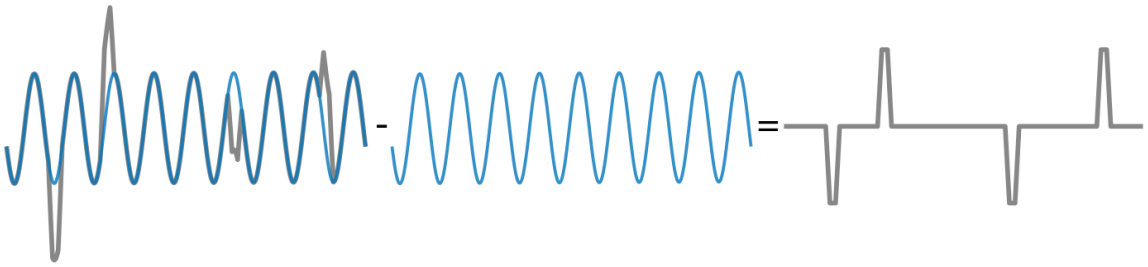

Figure 2.3: *Diagram of the perturbation response extraction technique. The response to the reference trajectory subtracted from the response to the perturbation-augmented reference trajectory yields the response to the perturbations alone.*

Each mass-spring combination case was matched to one of five reference torque trajectories, $\psi_{\text{A-E}}$, seen in (2.2),(2.3),(2.4),(2.5),(2.6). Each sine wave takes the form of $A\,sin\,(\omega t) + B$ where A is amplitude in Nm, ω is the frequency in Hz, t is the

time in seconds, and B is the torque offset is in Nm. The tested frequencies were chosen to encompass the known frequency of able-bodied human gait [57], previous dynamic impedance experiments [2], and the frequency of pathological gait [58, 59]. The case-trajectory combinations are referred to hereafter by the mass-spring combination (case numbers: 1-4) followed by the trajectory type (A-E) (1A, 3D, etc.).

$$\psi_{\mathrm{A}} = 5\,sin\,(1.4t) + 32 \tag{2.2}$$

$$\psi_{\mathrm{B}} = 5\,sin\,(0.8t) + 32 \tag{2.3}$$

$$\psi_{\mathrm{C}} = 5\,sin\,(2.0t) + 32 \tag{2.4}$$

$$\psi_{\mathrm{D}} = 6\,sin\,(1.4t) + 32 \tag{2.5}$$

$$\psi_{\mathrm{E}} = \frac{1}{2}\left[5\,sin\,(1.4t) + 6\,sin\,(2.0t)\right] + 40 \tag{2.6}$$

During testing, two forms of the five reference torque trajectories were supplied to the exoskeleton: the first form was the sine wave described above and the second form was the sine wave augmented with eight perturbations. The perturbations had a magnitude of seven Nm and their profiles consisted of a ramp of 75 ms, a 100 ms hold, and a negative 75 ms ramp to return to the torque trajectory. These perturbations were placed at 10%, 40%, 60%, or 90% of the sine wave corresponding to the middle of the loading phase, mid-terminal stance, toe-off, and the transition from mid to terminal swing phase of the gait cycle respectively. This perturbation paradigm has been used previously for validation of methods for estimating ankle stiffness using a robotic device [39]. We conducted seven trials at each reference trajectory, during which the output shaft position and torque from were measured at a sample rate of 900 Hz.

Perturbations were extracted by subtracting the exoskeleton's response to the non-perturbed sine wave from its response to the perturbed sine wave (2.3) [60]. Following extraction, isolated perturbations were segmented and analyzed in a 100-ms window following the onset of the perturbation. A least-squares algorithm was applied to fit a second-order impedance model to the data according to 2.1. Accuracy of stiffness and inertia estimates were assessed by comparing model-estimated values to the known mass-spring values and were quantified using percent error.

2.2.4 Statistical Analysis of Stiffness and Inertia Estimates

The statistical measures of variance accounted for (VAF) and analysis of variance (ANOVA) were performed on the estimates of stiffness and inertia. VAF is used to show how a model predicts the variance of measured data. 2.7 shows the equation for VAF where $T_{est}(t)$ is the estimated torque calculated from the estimated impedance parameters as a function of time and $T_{meas}(t)$ is the torque measured from the exoskeleton as a function of time.

$$VAF = [1 - \frac{\sum (T_{\text{est}}(t) - T_{\text{meas}}(t))^2}{\sum T_{\text{meas}}(t)^2}] * 100 \tag{2.7}$$

Four one-way ANOVAs were conducted on each case-trajectory combination to elucidate the effect of perturbation type (i.e: whether the perturbation was a positive or negative torque perturbation) and perturbation direction (i.e: if the perturbation was in the same or opposite direction of the underlying trajectory) on stiffness and inertia estimates. ANOVAs were performed using MATLAB and the p-values of case-trajectory combinations that did not show significance are reported in the results.

Table 2.1: *Average percent error and standard deviation of stiffness (K) estimates for each trajectory*

K Table	Trajectory A	Trajectory B	Trajectory C	Trajectory D	Trajectory E
K_1	3.73 ± 0.51	-2.54 ± 2.37	-5.14 ± 1.32	-2.44 ± 0.01	-1.27 ± 0.99
K_2	-0.28 ± 0.51	-0.49 ± 1.20	-12.70 ± 1.83	-0.16 ± 0.83	-0.94 ± 4.25

Table 2.2: *Average percent error and standard deviation of inertia (I) estimates for each trajectory*

I Table	Trajectory A	Trajectory B	Trajectory C	Trajectory D	Trajectory E
I_1	-1.80 ± 6.34	-11.5 ± 4.63	-30.2 ± 19.8	-11.0 ± 8.87	-19.6 ± 2.00
I_2	-12.9 ± 3.16	-9.32 ± 5.45	-22.7 ± 16.2	-7.31 ± 0.22	-15.1 ± 12.3

2.3 Results

2.3.1 Characterization of Exoskeleton Bandwidth and Intrinsic Impedance

The system bandwidth was found to be 26.8 Hz for the 20 Nm noise signal and 17.2 Hz for the 40 Nm noise signal (2.5). The average intrinsic stiffness, damping, and inertial components of the exoskeleton were found to be 0.388 ± 0.194 Nm/rad, 0.163 ± 0.0130 Nms/rad, and $0.00100 \pm 2.65\text{x}10^{-5}$ kgm^2 respectively. These intrinsic impedance values were subtracted from the measured external impedance values to yield the estimated external impedance values reported.

2.3.2 Dynamic Estimation of Mechanical Impedance

Averaged stiffness, damping, and inertia estimates for the five reference trajectories have been shown in 2.6. On average, errors for the stiffness estimates were $-2.15 \pm 3.49\%$ for k_1 and $-2.51 \pm 5.73\%$ for k_2. Average errors for the inertia estimates were $-15.2 \pm 10.91\%$ for I_1 and $-13.1 \pm 5.91\%$ for I_2. A Percent error breakdown of stiffness and inertia estimates by trajectory are in 2.12.2.

2.3.3 Statistical Analysis of Stiffness and Inertia Estimates

The VAF values for all case-trajectory combinations were above 99.9% with the exception of 4B, which had a VAF of 95%. The one way ANOVA results for most case-trajectory combinations produced a p-value under 0.05, showing that perturbation direction, perturbation type, or both had a statistically significant effect on stiffness and inertia estimates. Perturbation type was found to be a statistically significant factor for all stiffness estimates. The case-trajectory combinations where perturbation type was not statistically significant were 1C ($p = 0.835$) and 2E ($p = 0.754$) for inertia estimates. Perturbation direction was found to be a statistically significant factor for affecting impedance estimates with most combinations. The exceptions to this were 4C ($p = 0.469$) and 4D ($p = 0.190$) for stiffness estimates and 1A ($p = 0.826$), 2A ($p = 0.056$), and 4E ($p = 0.384$) for inertia estimates.

2.4 Discussion

The objective of this letter was to investigate the system identification capabilities of a torque-controlled knee exoskeleton for future applications of characterizing human knee impedance. Our methods included characterization of system bandwidth and intrinsic impedance and implementation of perturbation-based system identification techniques to estimate the mechanical impedance of external mass-spring systems. We chose system parameters that could best emulate human locomotion in a bench top setting. We were encouraged by our results. The system's minimum bandwidth, 17.6 Hz, was found to be significantly higher than what we would need to study human locomotion. The intrinsic impedance was found to be low in comparison to the tested systems. Estimated external impedance results were particularly encouraging: stiffness estimate errors were under 3% and inertia estimate errors ranged from ∼13-15%.

2.4.1 Stiffness and Inertia Estimates

The average stiffness and inertia estimates with our device are better than or equivalent to the state of the art. The average stiffness errors for the two tested springs (2.15% and 2.51%) were lower than the reported average stiffness errors of other systems designed for determining dynamic lower limb impedance (5% [2] and 15% for 13 of 18 trials [54]). The average inertia estimate errors from our system (15.2% and 13.1%) were comparable to those reported by Tucker et al. (15% for 16 of 18 trials [54]).

For most of the tested trajectories, we noted better estimates of stiffness and inertia at higher values of these parameters. The exceptions to this trend were the inertia estimates for trajectory A and stiffness estimates for trajectory C. Overall, impedance estimates were likely better at higher values because higher impedance more closely mimics the conditions under which the system was tuned: the system's torque controller was tuned by locking the output of the exoskeleton, which is analogous to attaching an infinite stiffness and large inertia to the exoskeleton.

Our stiffness estimates had a lower percent error than our inertia estimates. Stiffness estimates had both, lower maximum and minimum errors than the inertia estimates as well as tighter standard deviations. Segmenting measured torque according to 2.1 offers insight into why this might be: the $k\theta$ component of torque is larger than the $J\ddot{\theta}$ component. Alternatively, a larger error in estimating J error could be attributed to the numerical method used to determined velocity and acceleration, which tends to lose fidelity with higher order derivatives.

2.4.2 Statistical Analysis

Statistical analysis shows that the parameter estimates accurately model torque behavior and how perturbations are administered has an effect on impedance estimates.

VAF was high in all cases which was expected, because the second order relationship of mass-spring systems to torque is both well known and characterized. The ANOVAs indicate that how perturbations are applied matters. Over 91% of the ANOVAs showed that pertrubation type or direction has a statistically significant effect on the estimation of impedance parameters. A statistically significant effect was found 95% of the time for ANOVAs exploring perturbation type and 87.5% of the time for ANOVAs exploring direction. Further analysis showed when comparing the stiffness estimates of perturbations in the direction of the underlying trajectory to those that were not, we found that perturbations in the same direction as the trajectory were larger 75% of the time. Surprisingly, when comparing stiffness estimates based on perturbation type (positive or negative), positive perturbations only yielded larger estimates 55% of the time. We saw the opposite trends for inertia estimates with same direction perturbations and positive perturbations being larger 36.3% and 40% of the time respectively. This is expected because the system has no damper, resulting in an adversarial relationship between stiffness and inertia.

2.4.3 Experimental Implications

The results revealed that the frequency of the applied reference trajectory affects the quality of the resulting impedance estimate. Trajectories A, B, and D had frequencies ranging from 0.8-1.4 Hz, which fall under slow walking or pathological gait [58, 59, 2, 39]. Trajectories C and E had frequencies ranging from 1.7-2.0 Hz, which fall under able-bodied human gait [57]. We found that impedance estimates from trajectories at lower frequencies were more accurate, with lower stiffness and inertia estimate errors and damping estimates closer to zero. These results indicate that tight control of human gait frequency will be critical for quality data collection. We don't believe testing at slower gait speeds will negatively impact our results as previous work characterizing human joint impedance during locomotion, collected data at

gait frequencies much lower than the frequency of able-bodied human gait [32, 2, 39].

Our results have informed us about how we should conduct human experiments and how accurate we can expect the results to be. The data shows us that we should run experiments at lower frequencies to achieve the highest accuracy. Data also shows us that we can be confident in our estimates of stiffness and damping due to the low percent error readings. We know that measurements of dynamic stiffness are lower than their postural counterparts and so we believe that case 2 results may be like what we expect to see during human testing. Finally, these experiments have shown us that our estimates will likely be underestimates but we may be able to counteract this phenomenon by using perturbations in the same direction as the underlying trajectory for stiffness or perturbations in the opposite direction as the underlying trajectory for inertia estimates.

2.4.4 Limitations

Some limitations of this study must be considered. The bench top setup did not include an explicit damper and validation of the system identification capabilities of the device were limited to measures of stiffness and inertia. We did, however, report a damping estimate in our results. The average damping estimates were close to zero, which is an encouraging result for both, the device, and the system identification technique. Furthermore, estimates from 95% of the testing conditions had a standard deviation at least 1.4 times larger than the mean, indicating that the reading was dominated by noise. This illustrates the potential of this device to accurately measure human knee damping values in future studies. Another limitation to consider is that impedance estimates tended to fall below the true values. Inertia values revealed a notable skew towards underestimation of true values: inertia estimates for 100% of tested trajectories and 95% of the case-trajectory combinations were underestimates of the true value. Examining stiffness estimates by trajectory revealed that 80%

of the estimates fell below the true value. Examining stiffness estimates by case and trajectory, however, revealed that only 35% of the estimates fell below true values. We conclude that while inertia estimates were skewed towards underestimation, stiffness estimates were not strongly skewed in a single direction. Underestimation could be attributed to inherent variation in the torque applied by the exoskeleton: in a prior study characterizing the exoskeleton, output torque varied by up to $\sim$10%. This may arise from inaccuracies in the beam spring stiffness equation or from nonlinearities of the beam spring that are not captured by the linear model we have used. Overall, the accuracy of impedance estimates reported here, particularly for stiffness and damping, indicate that this issue can be overcome.

2.4.5 Ramifications of Human Experiments

With validation of the system identification capabilities of the device and the proposed methodology, we now have a reliable tool that can be used to further rehabilitative practices, prosthetic design, and robotic control. With a device that can determine knee impedance values for physically impaired and able-bodied individuals alike, we can use impedance as a metric for rehabilitation. Knowing how an individual's joint impedance varies after a medical intervention or rehabilitative session can be a tool for bench marking patient progress. Knowledge of how impedance varies can also be used for intelligent design of passive or quasi-passive prosthetic devices. Work presented in [12] shows how biological data can be used to design quasi-passive devices that perform comparably to their powered counterparts but show notable savings in weight and complexity. Using a similar approach with knee impedance data could prove beneficial in informing design requirements for the next generation of passive or quasi-passive knee prostheses. Finally, task-based knowledge of knee impedance provides opportunities for new control methodologies. Using our approach, we can definitively replicate the impedance of human joints on these powered devices and

compare their performance to other control laws. Experiments like this can inform the merit of exploring biological impedance for robotic control and could lead to more intuitive control and higher device adoption.

Acknowledgment

This work was supported by NSF grant number DGE 1256260 and NSF award number 1846969. This work was published in the ASME Journal of Biomechanical Engineering

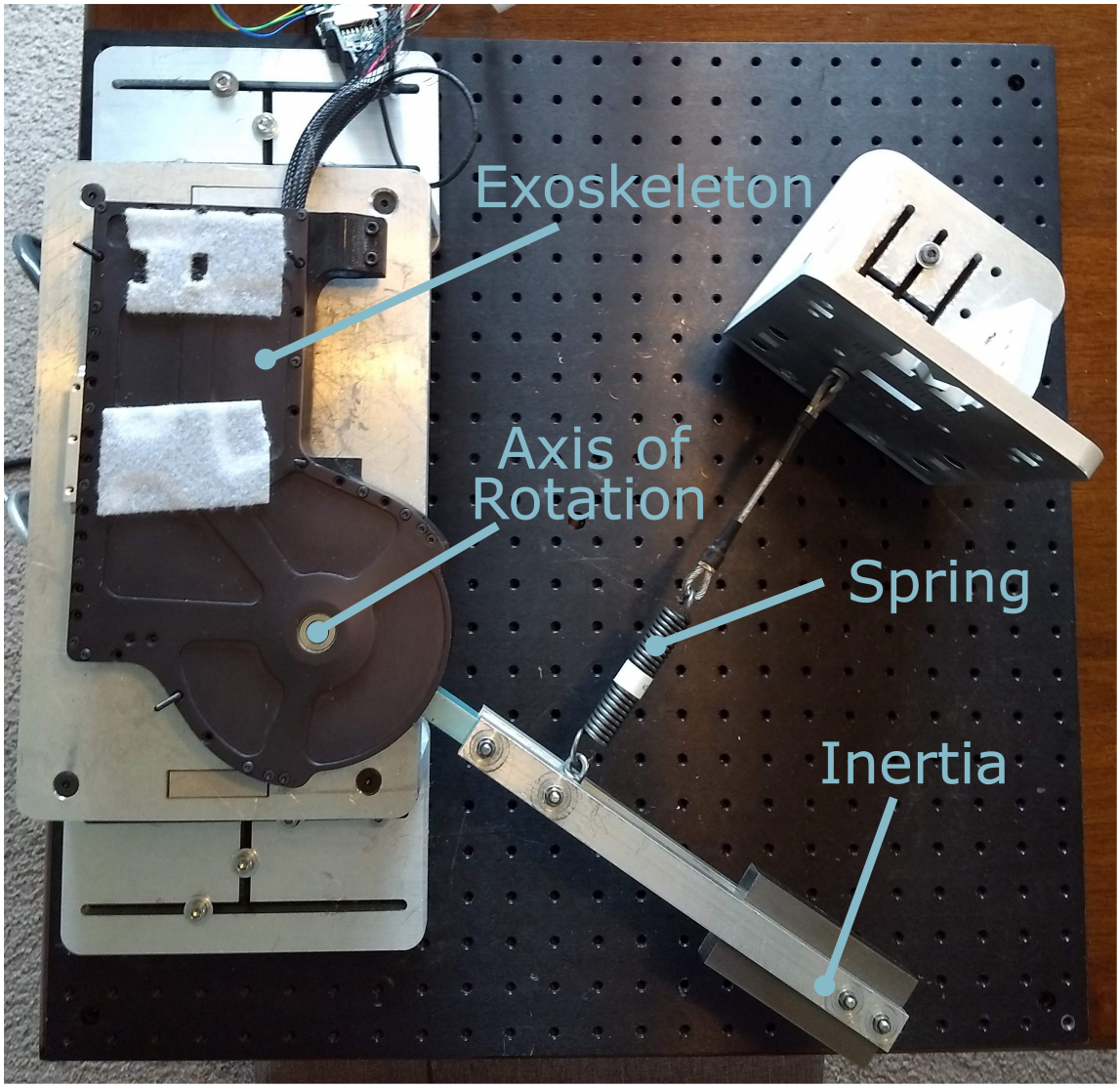

Figure 2.4: *Diagram of the experimental setup. Labeled components are the actuator and its axis of rotation, the spring and the inertia.*

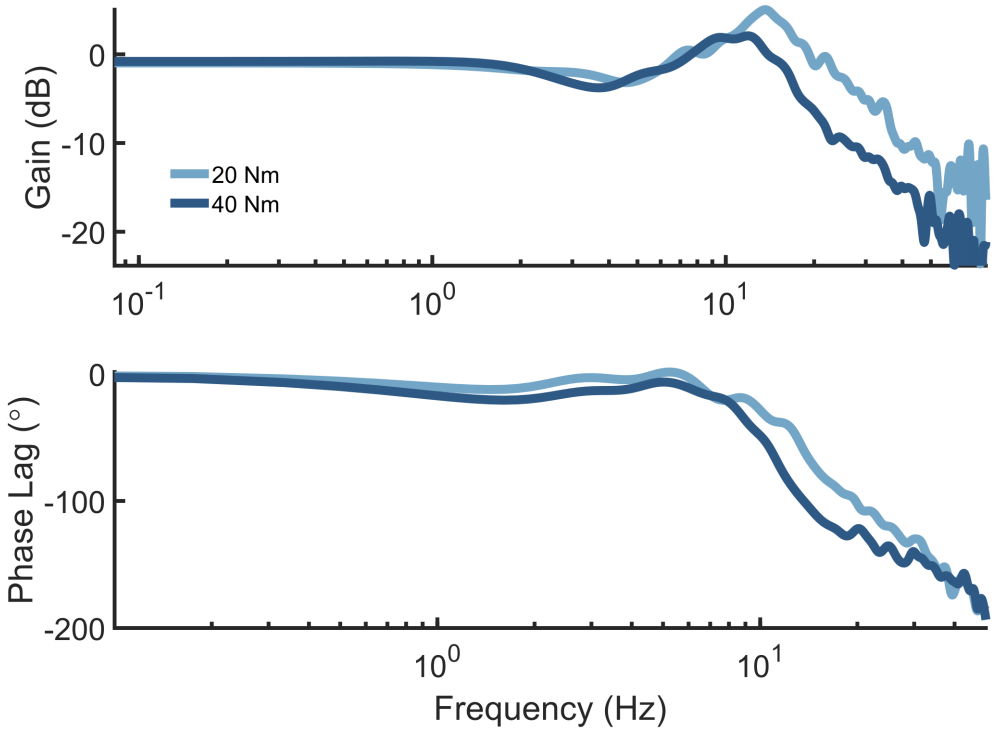

Figure 2.5: *Plot of the actuator's torque bandwidth at 20 and 40 Nm. Bandwidth was determined by measuring the system's torque response to a filtered Gaussian white noise (FGWN) signal with a cutoff frequency of 30 Hz.*

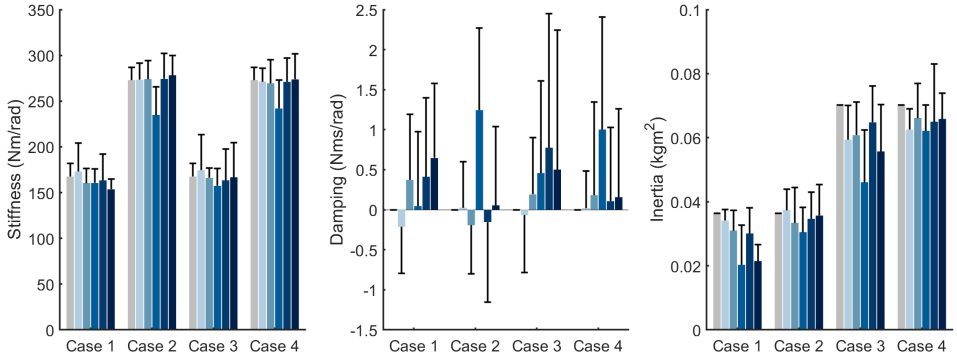

Figure 2.6: *Plot of average estimated stiffness, damping, and inertia values for all case-trajectory combinations. The ideal stiffness, damping, and inertia values are shown in gray. The experimental estimates of these values from tested trajectories are shown in shaded color, with the lightest color corresponding to Trajectory A and the darkest color corresponding to Trajectory E. Standard deviations are symmetric about the mean value.*

CHAPTER III

Characterization of a Quasi-Direct Drive Knee Perturberator For Human System Identification

3.1 Introduction

Understanding the mechanical impedance of human joints is necessary for a comprehensive understanding of movement. Mechanical impedance dictates how the body responds to disturbances and governs the exchange of energy between limbs during activities [61]. Mechanical impedance, in this context, refers to the relationship between an input flow or its derivative, i.e. position or velocity, and output an effort, like torque or force [15, 62, 63]. Knowledge of impedance has been used to create innovations in many subject areas, such as robotic control, mechanical design, and rehabilitation ([64, 65, 66].

Joint impedance is studied under static or dynamic conditions and while impedance in static conditions is well researched, knowledge of how impedance behaves in dynamic domains is not as plentiful. In the lower limbs, static impedance research has been conducted at all three major joints (hip, knee, and ankle) under a myriad of conditions, forming the foundation for most of the impedance research ongoing today [18, 11, 67, 23, 24, 25, 26, 27, 19, 20, 21, 22]. More recently, it has been shown

that there is a notable difference between joint impedance estimates obtained under static and dynamic conditions, leading to more studies under dynamic conditions [29]. Most of these dynamic studies have been conducted at the ankle, and out of these studies an interesting trend has emerged: studying impedance during common tasks [28, 29, 30, 16, 68, 69, 66]. Studying impedance during these common tasks provide insights into our execution of everyday activities such as walking or running, offering a more accurate depiction of how our joints function during these motions and thereby contributing to a more comprehensive understanding of human movement [29, 68, 69, 34, 35, 16].Equivalently important to the context in which we study impedance, is ensuring we possess devices that can capture the requisite information for impedance estimation during these dynamic tasks.

Exoskeletons serve as versatile tools for assessing mechanical impedance due to their adaptability in introducing perturbations during both the stance and swing phases of human movement [68, 70, 71]. This modality is critical for measuring joint mechanical impedance, as perturbation application to the joint of interest must occur for proper identification the closed loop system [67]. When employing an exoskeleton for system identification, it is essential to select a system that exerts minimal influence on the wearer's natural gait. Achieving this goal involves opting for actuation mechanisms with low weight, compact transmissions, and low interaction torques at the output. The integration of quasi-direct drive (QDD) actuators has emerged as an effective strategy for actuators that not only reduce mass, but also generate low interaction output torques efficiently [72]. The adaptability of these devices for general purposes is promising, however the efficacy QDD's as human system identification tools is unclear.

In this paper, we implement a QDD actuator as a system identification tool for quantifying the mechanical impedance of the knee joint during walking. First, a novel

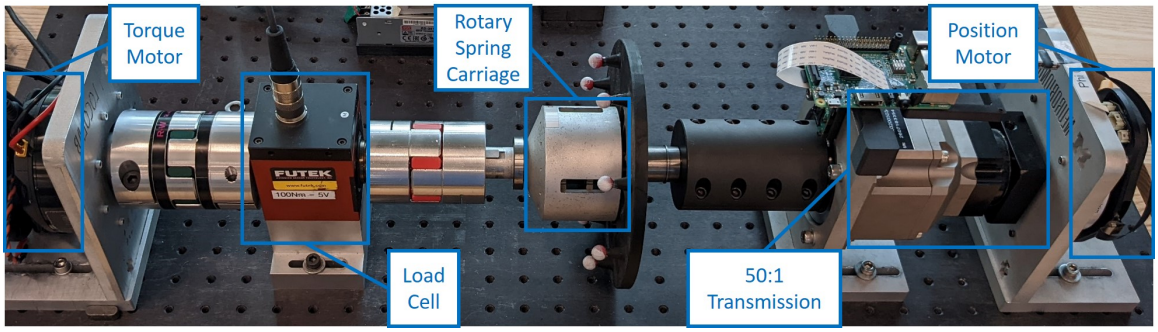

Figure 3.1: *Experimental test bench used for torque model testing and validation as well as static and dynamic mechanical system identification experiments.*

model for estimating torque exerted by the actuator is formulated using motor state information. We then investigate this model's torque measurement accuracy through a testing sequence where the model results are compared to a ground truth torque sensor measurement. Subsequently, the device's ability to identify the stiffness of a mechanical system is described under both static and dynamic conditions. Lastly, we conduct a perturbation experiment on two human subjects for the purpose of estimating knee joint mechanical impedance during walking. The reported values provide new mechanical impedance information during the swing phase of gait, as well as the first insight into the mechanical impedance of the knee joint during the stance phase of walking. This work not only helps establish the ability for QDD actuators to measure system dynamic properties, but also demonstrates how the actuator can be integrated into future exoskeleton systems for the purpose of human impedance identification.

3.2 Methods

In order to assess the actuator's capacity for estimating mechanical impedance parameters, we conducted experimental procedures on a bench top testbed featuring a torque motor and a torque sensor coupled to rotary springs 3.1. The testbed consisted of a motor on the left side that operated in current control, denoted the *torque motor*

(9:1 ActPack, Dephy Inc, Boxborough, MA). The torque motor was coupled to a torque sensor (TRS605, Futek, Irvine CA) which was fixed to two 150 Nm/rad rotary springs in parallel from [73]. The rotary springs were connected to a transmission (50:1 PL2090-050, Boston Gear, Boston MA), the input of which was mounted to a motor that operated in position control, denoted the *position motor*. To determine if the actuator was capable of performing system identification adequately, we first needed to validate the system's ability to estimate torque.

3.2.1 Identification of Open-Loop Actuator Torque Model

We conducted a test that commanded a series of constant velocities from the position motor and constant torques from the torque motor to fit the parameters within a model to estimate motor torque. The torque and speed test was conducted with the torque side motor holding seven different levels of torque that ranged from -10 to 10 Nm while the position side motor proceeded through six different velocities ranging from negative five to positive five rad/s. The resulting torque side motor data was fit to three different torque models using least squares regression. Model 3.1 estimates torque, τ, using a bias term, ϕ, the motor's transmission ratio, g_r, a torque constant, k_t, and q-axis motor current, I_q. Model 3.2 used a traditional motor equation to estimate output motor torque, using a bias term, the motor's transmission ratio, torque constant, q-axis motor current, the motor's viscous loss, b, and the motor's rotor inertia, J. The torque estimation model we proposed can be seen in 3.3 where the output torque is characterized by the bias in the torque sensor, the gear ratio of the motor, the torque constant of the motor, the q-axis current drawn by the motor, the motor's coulomb friction, f_c, the motor's velocity, $\dot{\theta}$, the gear friction in the motor, f_g, the rotor inertia of the motor, and the motor's acceleration, $\ddot{\theta}$. J for model 3.3 was extracted from previous work involving this actuator [72]. The RMS error of each model was calculated and used to determine model efficacy. The model with the

lowest RMS error, would be validated through further experimentation.

$$\tau = \phi + g_r k_t I_q \tag{3.1}$$

$$\tau = \phi + g_r k_t I_q - b(\dot{\theta}) - J\ddot{\theta} \tag{3.2}$$

$$\tau = \phi + g_r k_t I_q - f_c sign(\dot{\theta}) - f_g |I_q| sign(\dot{\theta}) - J\ddot{\theta} \tag{3.3}$$

We wanted to investigate the torque tracking accuracy of the model with the lowest RMS error in the presence of disturbances. To perform this task, we had the torque motor produce a series combination of chirp signals with various amplitudes. To provide a disturbance for the torque motor, we had the position motor produce a series combination of chirp signals as well. The torque series combination of chirp signals consisted of four chirp signals. The first chirp had an amplitude of five Nm, followed by seven Nm, 10 Nm, and finally zero Nm. Each chirp signal started at a frequency of one Hz and increased to 10 Hz. Each torque chirp lasted for a duration of 10 seconds, making the duration of the series combination of signals 40 seconds. The position series combination of signals consisted of one chirp signal that repeated four times. The position chirp started at a frequency of 10.1 Hz and an amplitude of five degrees. This signal decreased in frequency and amplitude to 1.1 Hz and three degrees, respectively. Each position chirp lasted for a duration of 10 seconds, making the duration of the series combination of signals 40 seconds. The torque and position series combination chirp signal were started simultaneously, and ran concurrently. To acquire a measure of torque tracking accuracy, we calculated torque using the minimum error model and compared those values to the readings from the testbed

torque sensor using RMS error as a metric.

3.2.2 Impedance Identification of Test bench System Under Static Conditions

Following determination of the torque model with the lowest RMS error, we conducted an experiment to quantify the actuator's ability to identify the stiffness of a mechanical system in a static configuration. To this end, we performed a test where the torque side motor sinusoidally commanded a range of -10 to 10 Nm six times in 60 seconds while the position output was locked. The torque side motor's encoder was used to measure the deflection of the mechanical system. A ground truth torque was measured from the torque sensor 3.1. From the torque and motor position data, the true stiffness of the system was estimated. The estimated system stiffness was calculated using the torque model and motor position data. The stiffness estimates were compared to the ground truth measurements using percent difference.

3.2.3 Characterization & Impedance Identification of Test bench System Under Dynamic Conditions

In addition to characterizing the stiffness of the mechanical system in static conditions, a separate experiment was used to estimate the stiffness in dynamic conditions, that would more closely mimic testing during human locomotion. To identify the stiffness of the mechanical system under dynamic conditions, we performed an independent characterization of the system that we will refer to as the IDP test moving forward. For this characterization, the position side motor followed the trajectory $3sin(\pi x/5) + sin(10\pi x)$ degrees, while the torque side motor commanded the following torque trajectory $10sin(\pi x/5)$ Nm for 60 seconds. We filtered the data at a frequency of $\sqrt{5}$ Hz to remove the high frequency behavior in the resultant signals and regressed the data to determine the dynamic system stiffness.

To evaluate the actuator's ability to estimate mechanical impedance under conditions akin to human experiments, a perturbation experiment was performed under dynamic conditions. The position side motor in the perturbation experiment followed the knee position trajectory from a reference dataset at a speed of 1 m/s [74]. The torque side motor enacted two conditions. First condition was the *no perturbation condition* (NPC) where the torque side motor followed a zero torque reference signal. The second condition was the *applied perturbation condition* (APC). During this condition, the torque motor would cyclically track a zero torque reference signal for 2.75 seconds and then apply a 250 ms perturbation. The perturbation consisted of a 75 ms ramp up from zero to seven Nm, a 150 ms hold at seven Nm, and then a 75 ms ramp down from seven to zero Nm. The perturbations applied alternated between being applied in the positive and negative torque directions, with 20 perturbations being applied in total. The NPC condition occurred for 60 seconds. Promptly after the NPC condition, the APC condition occurred for 60 seconds. The torques applied and position traversed by the torque side motor for both the NPC and APC cases were sectioned into individual "gait cycles." Once the torque and positions from each gait cycle were segmented, the torque and position trajectories from the NPC case were subtracted from the APC case to isolate the system's impedance response. After the isolated system responses where found, system identification methods were used to determine the system stiffness. This stiffness was compared to the independently determined stiffness of the system. From this comparison percent error was calculated.

3.2.4 Human Impedance Estimation Pilot Experiment

An altered version of the methods previously stated for impedance estimation during dynamic conditions were applied on N=2 able-bodied subjects (gender: 1 female/-male, mean age: 23 $\pm$0.00, mean mass: 72.58 $\pm$9.08 kg). Prior to data collection, subjects gave informed consent to a protocol approved by the University of Michigan

Institutional Review Board. Each subject underwent two walking conditions while wearing a knee exoskeleton; an exoskeleton no perturbation condition (E-NPC) and an exoskeleton applied perturbation condition (E-APC) 3.2. All conditions occurred on a treadmill at a speed of 1.2 m/s. The E-NPC condition was conducted for approximately 60 gait cycles, while the participants walked as the exoskeleton tracked a zero torque reference trajectory about the knee joint. During the E-APC condition, participants received perturbations at six time points within the gait cycle, while between perturbations, the exoskeleton tracked a zero torque reference trajectory. These time points correspond to the loading response, mid-stance, terminal stance, pre-swing, initial swing, and mid-swing phases of gait outlined in [75]. There were 50 perturbations applied at each time point in the direction of knee flexion. Perturbation onset occurred at the time point that corresponded to 50% completion of a specific phase of gait. Each perturbation was a 17 Nm torque hold, applied for 250 ms. Subjects were randomly perturbed every three to seven gait cycles. Torque information was calculated offline using model 3.3. The joint position information was collected using an electrogoniometer across the knee joint (MLTS700, AD Instruments, Colorado Springs CO). Mechanical impedance parameters were determined using similar system identification methods to previous work [76]. For the E-NPC and E-APC cases, the torque and position information from each individual gait cycle was segmented. For the E-NPC case, all torque and position information from individual gait cycles were averaged to produce a mean torque and position trajectory. All E-APC gait cycles where a perturbation occurred were sorted by the timing point at which the perturbation occurred. The average gait cycle torque and position information from the E-NPC case was subtracted from each E-APC gait cycle to remove the underlying torque and position that result from walking, thereby isolating the perturbation and response. The isolated torque and position perturbations were then used with least squares identification to determine stiffness (K), damping (B), and inertial (J) values

that parameterize second-order mechanical impedance models. Reported impedance parameters K and B were normalized by subject weight and all parameters (K, B, J) were averaged. The Variance Accounted For (VAF) resulting from each subject's regressed impedance parameters was quantified. VAF provides a measure of how well the model fit the experimental data.

3.3 Results

3.3.1 Identification of Open-Loop Actuator Torque Model

The model parameters estimated from the multi-regime torque-speed test yielded similar results for shared parameters, such as ϕ and k_t, but had different RMS errors. The regressed parameters and RMS error for each model are in table 3.1. Model 3.3 was used to estimate torque for subsequent experiments because it provided the lowest RMS error. The RMS error from the chirp validation test was 0.33 Nm with model 3.3.

Table 3.1: *Torque-Speed Model Parameters and RMS Torque Errors*

Model Type	Parameters	RMS Torque Error (Nm)
1	ϕ = -0.58, g_r = 9, k_t = 0.11	0.88
2	ϕ = -0.57, g_r = 9, k_t = 0.11, b = 37e-4, J = 0.22	0.44
3	ϕ = -0.58, g_r = 9, k_t = 0.11, f_c = 0.38, f_g = 0.09, J = 92e-4	0.38

3.3.2 Impedance Identification of Test bench System Under Static Conditions

Under static conditions, the estimation approach was able to accurately identify the stiffness of the included spring. Estimation of the stiffness coefficient yielded a sub one percent error. When compared to an independently-determined ground truth value, our estimation approach determined the stiffness within 0.81%.

3.3.3 Characterization & Impedance Identification of Test bench System Under Dynamic Conditions

Our estimation method correctly identified the stiffness of the benchtop system with approximately 5% error. The IDP test performed to identify the system stiffness under dynamic conditions yielded a result of 146.39 Nm/rad. The perturbation experiment conducted to identify the system stiffness under dynamic conditions produced an average error of 5.29% when compared to the independently identified stiffness coefficient. The perturbations in the positive direction yielded an estimated stiffness of 145.13 ± 2.45 and the perturbations in the negative direction yielded an estimated stiffness of 162.57 ± 2.96.

3.3.4 Human Impedance Estimation

Knee stiffness, damping, and inertia show their own unique trends as the gait cycle progresses, with stiffness being highest at the beginning of gait, damping being relatively level, and inertia being the highest during the middle of the gait cycle. The individual and average impedance estimates of the two human participants are shown in 3.7. Average stiffness results ranged from 2.99 to 0.11 Nm/rad/kg, average damping results ranged from 0.06 to 0.04 Nms/rad/kg, and average inertia results ranged from 0.05 to 0.01 kgm^2. The average VAF's for each subject across all timing points were 97.83% and 84.84% for subjects 1 & 2 respectively. The average VAF for both subjects was 91.3%.

3.4 Discussion

Through a collection of experiments, we explored the utility of using a compact, quasi-direct drive actuator for estimating the mechanical impedance of mechanical and biological systems. We first investigated the ability to model the actuator torque

using motor state information. We then validated this model's performance by performing a torque tracking test where we found the error of this model to be less than 0.5 Nm. Next, we used the best performing torque model to estimate the stiffness of a mechanical system under static and dynamic conditions. Finally, we applied techniques similar to those used to estimate the mechanical properties, to estimate the mechanical impedance of the knee joint for two human participants during walking. With this work, we provide new insight into the properties of the human knee during the stance and swing phases of walking.

Device characterization show that our actuator performs at a level equivalent to or superior than other state of the art perturbation devices. Our torque modeling error of 0.33 Nm is commiserate with the results of the MIT Anklebot which reported a sub one Nm torque tracking error [77]. Our stiffness estimates are on par with values reported from other work. For devices that apply perturbations in the sagittal plane, literature shows that these devices can estimate stiffness within errors ranging from 1.68% to 15% [34, 78, 30]. The device with the lowest stiffness estimate error we found in literature came from Ficanha's work. This study displayed an error of 0.15% from perturbations applied in the frontal plane [78]. All of the estimates from literature were performed under static or quasi static testing conditions. Our stiffness estimate error of 0.81% under static testing conditions is a strong result when compared to the field. Furthermore, our stiffness estimate error of 5.29% under dynamic testing conditions is a quality result amongst the results from other static studies, which undergo less complex dynamics.

Exoskeletons as perturbation devices provide alternate perturbation opportunities and drawbacks not afforded by recessed platform perturberators. One of the benefits of using an exoskeleton is that one can perturb participants during swing phase which cannot be accomplished with a recessed platform. Swing phase is integral com-

ponent of gait and knowledge of how impedance varies during this time can have major repercussions for robotic control, particularly in the field of prosthetics [10]. Using exoskeletons as perturbation devices opens the possibility of testing a new set of timing points that were previously neglected by recessed platforms. However, an additional consideration when using exoskeletons for impedance estimation during swing, is the effect the device has on user gait. If the device is too heavy or has high output impedance, the underlying biomechanics can be notably effected, calling into question the validity of the results. Another benefit of exoskeletons is the increased number of perturbations that can be applied, when compared to recessed platforms, given the same duration of time. Exoskeletons provide the ability to perturb multiple times during a single gait cycle which can lead to quicker experiments or more dense data sets for experimenters. Lastly, exoskeletons provide the ability to apply torque directly at the joint of interest, while platforms must use an inverse model to calculate the torque at that joint. Due to variations in foot placement during platform experiments, inverse models may experience inconsistent center of rotation calculations which impacts the estimation of torque and impedance at the joint of interest [34]. While exoskeletons do not experience this issue, problems can arise with torque transmission to the joint because of poor interface connections or human soft tissue. Taking these factors into consideration when performing perturbation experiments is important, and likely some combination of both approaches will yield the best results.

The stance phase knee impedance estimates in this paper are, to our knowledge, the first of their kind, and our swing phase estimates provide new data points, not yet seen in literature. During the loading response, mid, and terminal stance phases, we see stiffness and damping exhibiting antagonist behaviors with stiffness decreasing as damping increases. This behavior mimics a pattern seen at the ankle in previous literature [61, 69]. During this period of gait, we also see inertia increasing. During the initial and mid swing phases, our stiffness estimates lie in the range of previously

reported values and our inertia estimates closely align with previously reported data [16, 30]. Our damping estimates, however, are much larger than those reported in literature. For one the two studies that previously report this information, we believe this is because their time window for analysis is much longer than ours (275 ms compared to our 100 ms). This much longer time window allows reflexes to have a large impact on the total impedance of the joint which could explain the difference [79]. The other paper uses the same time analysis window as us, however their average VAF value is $\sim 72\%$ which is lower than ours at $\sim 91\%$. We believe the difference in model fits may explain this discrepancy between damping estimates.

3.4.1 Limitations & Future Work

The results of this work are shaped by key assumptions and limitations of the experimental setup. One key assumption made in this work is that the joint undergoes linear time invariant behavior during our time analysis window. The other is that knee joint impedance exhibits second order behavior. Previous literature has shown that representing human joints as second order, linear time invariant systems can account for more than 97% of model variance, providing us confidence in our assumptions [67]. Two limitations of this work are the sample size of the human experiment and a dearth of knowledge of the exoskeleton's effect on subject gait. We only tested two subjects in this work, which does not allow us to confidently make any statistical claims our impedance estimates. Any continuation of this work, should include an increased number of subjects in an effort to study a more globally representative sample of people and to confidently make statistical claims about their impedance estimates. Future work should also investigate the effect that wearing an exoskeleton has on participant's gait. During our experiment, the participant gait visually appeared similar. However, more thorough inspection of participant's biomechanics should be performed to provide a increased understanding of the applicability of these

results to typical abled-bodied gait.

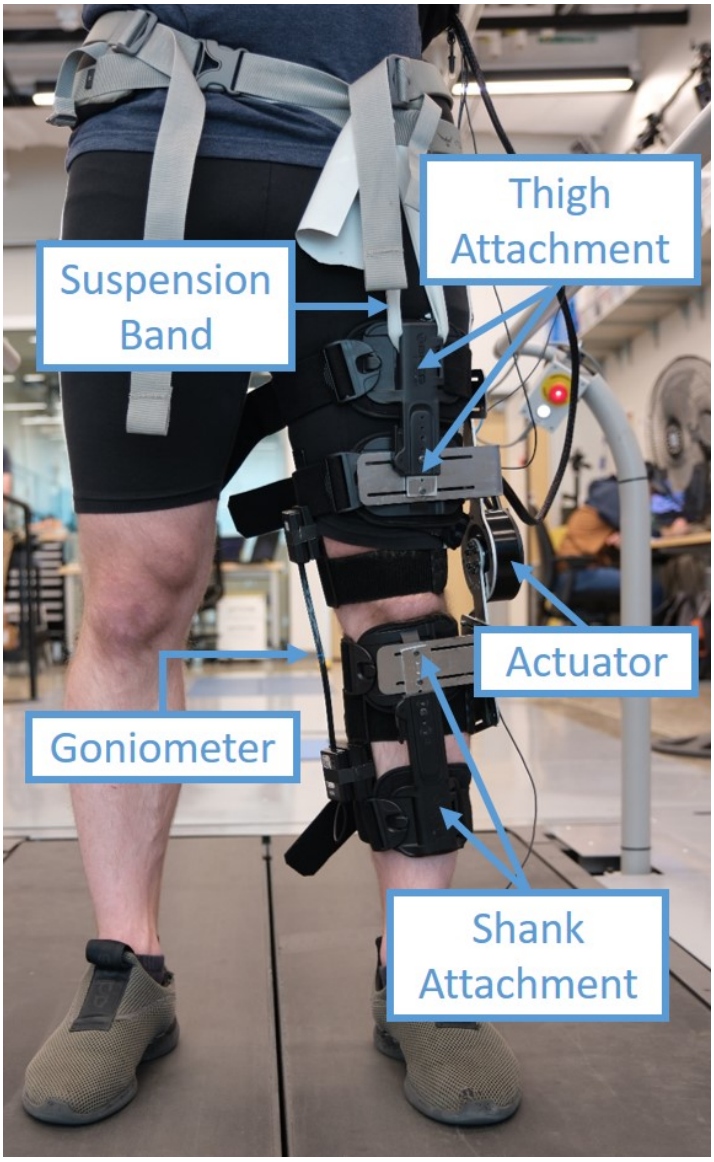

Figure 3.2: *Labeled figure of the exoskeleton used for human experiments. The torque side motor is labeled "actuator" in the figure.*

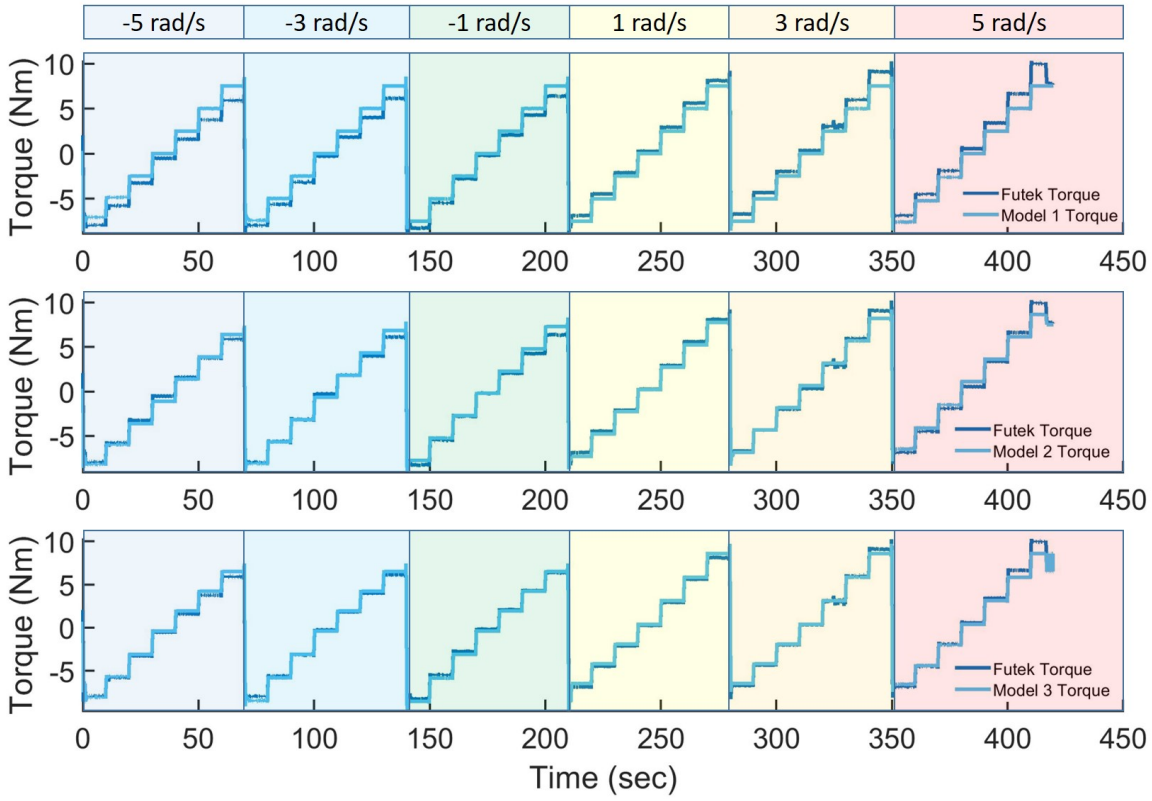

Figure 3.3: *Visualization of the performance of the three regressed torque models in comparison to a torque sensor. Colored legend shows the speed regime that each torque test is performed at.*

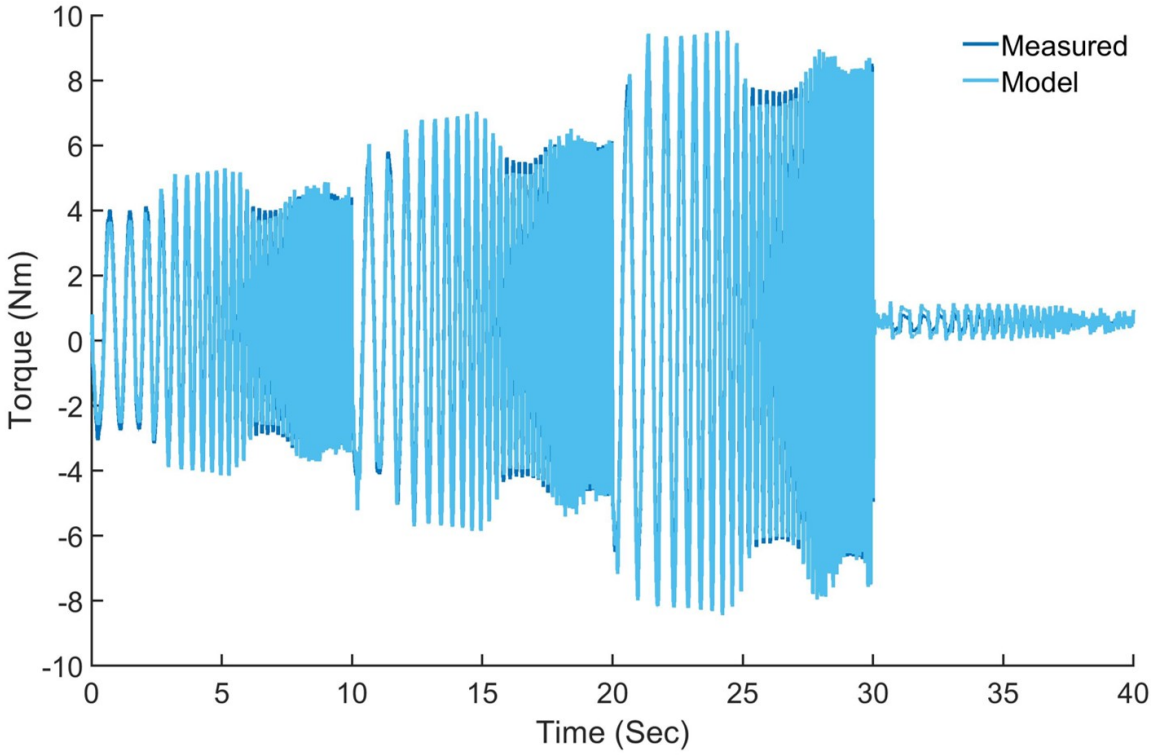

Figure 3.4: *Torque chirp validation test showing torque tracking of our model (model 3.3) vs the torque sensor at four different torque values.*

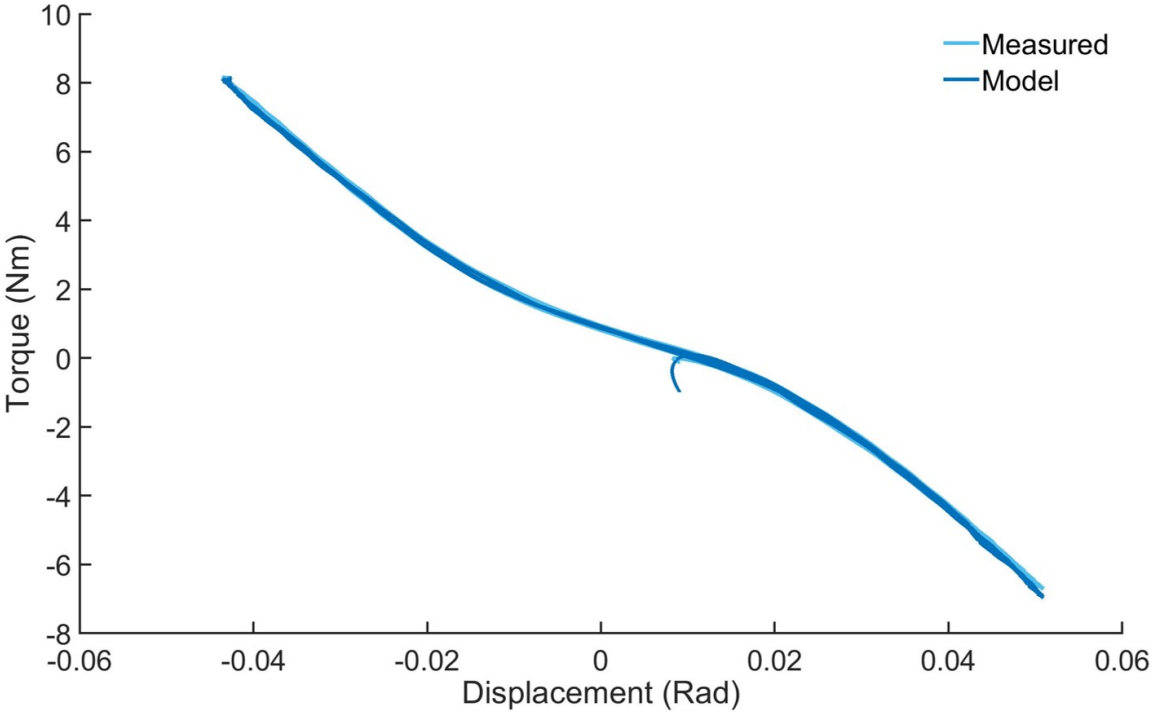

Figure 3.5: *Static system stiffness identification test. A 10 Nm amplitude sine wave was commanded by the torque side motor while the position output was locked in place.*

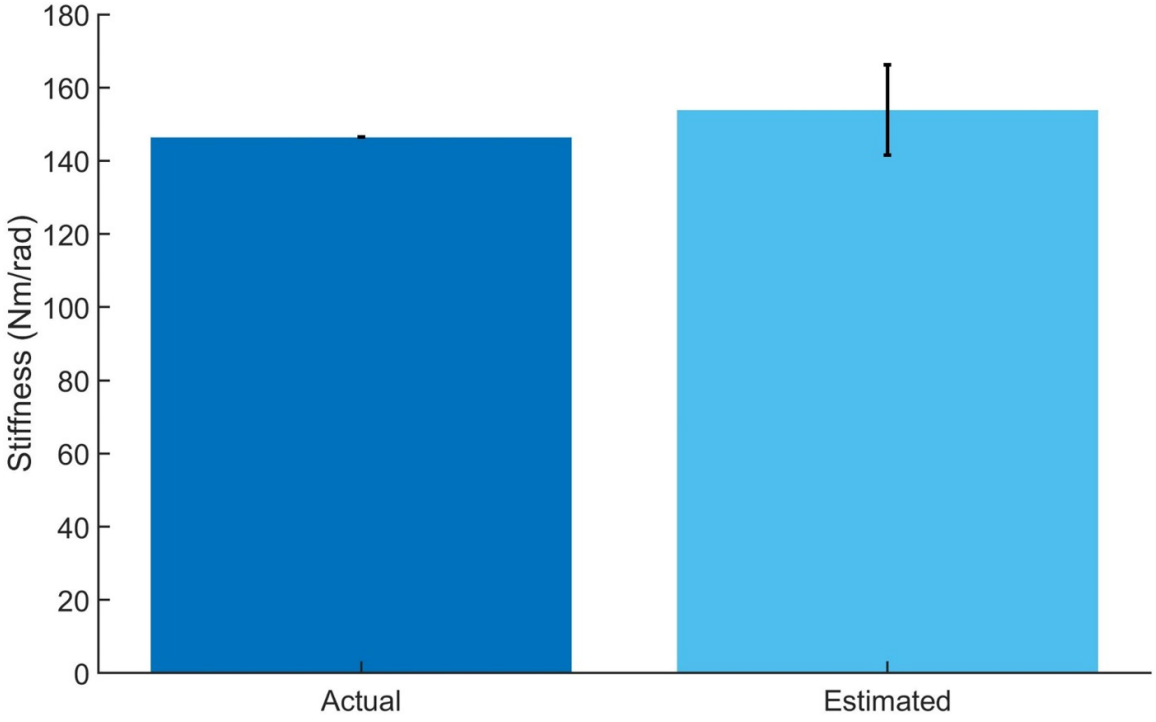

Figure 3.6: *Dynamic system stiffness identification result showing the difference in estimated stiffness from the perturbation experiment and the independent dithering test dynamic characterization.*

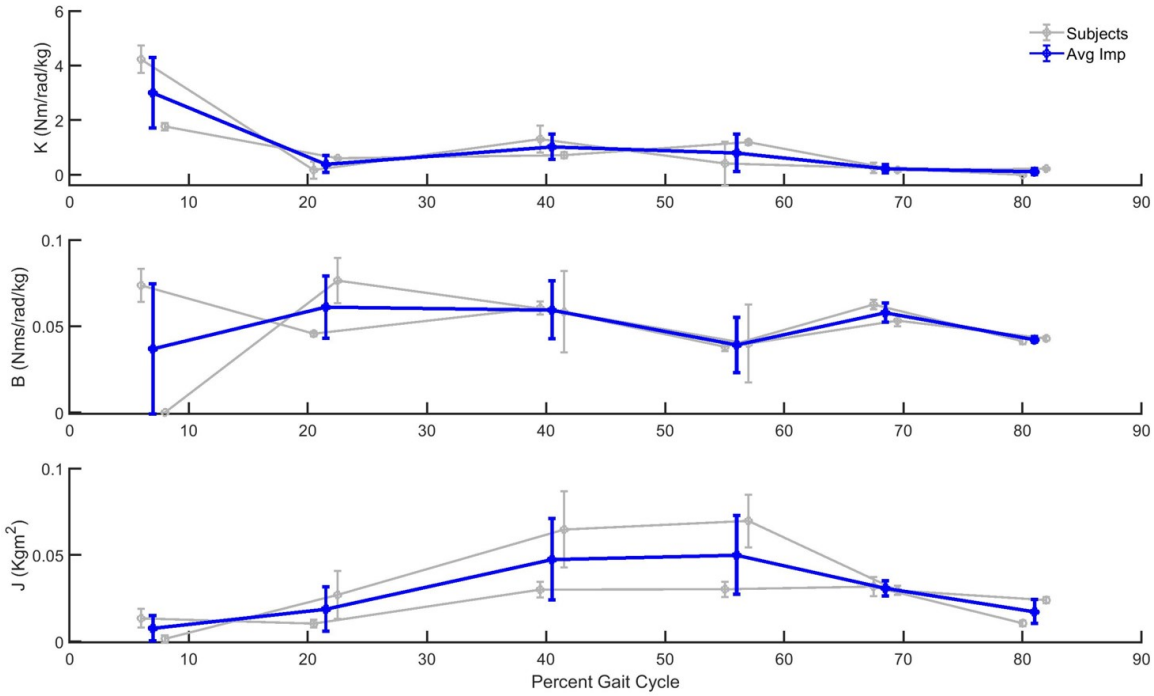

Figure 3.7: *Knee impedance estimates from two subjects during walking. Subject data is offset for clarity. Subjects were perturbed at six phases of the gait cycle and knee joint impedance was estimated at these points. Top shows stiffness normalized by mass, middle shows damping normalized by mass, and bottom shows inertia.*

CHAPTER IV

Estimation of Human Knee Joint Impedance During Walking

4.1 Introduction

Comprehending how mechanical impedance is exhibited by human joints is essential to gain a holistic insight into human motion. Mechanical impedance determines how the body reacts to perturbations and regulates the transfer of energy between limbs during various activities [61]. Mechanical impedance is defined as the relationship between an input position or velocity and an output force or torque [15, 62, 63]. Knowledge of impedance has led to breakthroughs in diverse domains, such as robotic control, mechanical design, and rehabilitation [64, 65, 66].

The human body regulates impedance based on environmental and situational factors. While impedance has been extensively researched under static conditions, our understanding of how impedance behaves in dynamic situations is relatively limited. For the lower limbs, a multitude of research has been conducted at major joints like the hip, knee, and ankle during static conditions, forming the basis of most current impedance knowledge [18, 11, 67, 23, 24, 25, 26, 27, 19, 20, 21, 22]. Recent studies have highlighted significant differences in joint impedance estimates during static and

dynamic conditions, prompting a shift towards more dynamic studies [29]. Amongst the dynamic studies, a trend in examining impedance during everyday tasks like walking or running can be seen [28, 29, 30, 16, 68, 69, 66, 80]. Analyzing impedance during these tasks offers valuable insights into how our joints function during dynamic actions, contributing to a more accurate understanding of human movement [29, 68, 69, 34, 35, 16]. Equally important as the context of impedance study is the need for devices capable of capturing essential information for impedance estimation during these dynamic actions.

To measure joint impedance there must exist a device that can apply perturbations to a subject without inhibiting their motion, and there must exist some tool for measuring the displacement of the joint and the torque about the joint as a result of the perturbation [67]. There are multiple types of devices that meet this criteria, and choosing which device to utilize will affect what aspects of impedance can be captured. One system that permits impedance estimation during dynamic tasks is the recessed force platform [34, 35, 36, 37]. Recessed force platforms are commonly operated in concert with a displacement measurement system, such as motion capture or an electrogoniometer, to gather impedance information. A caveat of recessed platforms is that the participant's foot must be in contact with the platform to apply a perturbation. This results in an inability to estimate impedance during activities, or segments of activities, when the subject is not contacting the ground, such as the swing phase of walking. An approach that addresses the foot contact limitations of recessed force platforms, is the utilization of a traction system [38, 16]. These traction systems employ external cables and motor-driven mechanisms to exert a linear force upon the subject. An advantage of these systems is their ability to administer perturbations to users regardless of if the target joint is in contact with the ground. However, a notable drawback of these systems are their complex system dynamics. Issues such as bowden cable bending or cable slack, can result in

discrepancies between the expected and actual forces experienced by the user.

Exoskeletons are versatile devices that show promise as effective tools for evaluating mechanical impedance. They enable the introduction of perturbations during both the stance and swing phases of human movement and have the capacity to apply torque directly to the joint of interest [68, 70, 71]. When utilizing an exoskeleton for system identification, it is imperative to select a system that minimally interferes with the wearer's natural gait. This necessitates choosing actuation mechanisms characterized by low weight, compact transmissions, and low output impedance. The integration of quasi-direct drive (QDD) technology into exoskeletons has emerged as a promising approach for reducing actuator mass and generating low output impedance [72].

The two most prevalent impedance estimation methods in the literature are experimental and model based. The experimental approaches utilize a device to perturb subjects and measure the kinetics of their response. At the knee, there are two documented approaches that use experimental perturbation methods. One is Kooij's work that estimated hip and knee impedance during the initial, mid, and terminal swing phases of gait with a pulling traction perturbation device [16]. The other is Tucker's work which estimated knee impedance during 20% and 30% of swing with an exoskeleton perturbation system [30]. The current state of the art works for model based estimates of knee impedance during walking consists of two studies. The first work comes from Pfeifer where they estimated knee stiffness during walking using an EMG based approach and the second is Sartori's work where they estimated ankle and knee stiffness during fast walking and running using a musculo-skeletal model [81, 48]. Both works use surface EMG, Ground Reaction Force (GRF) data, and motion capture information as the inputs for their model based approaches. In both studies, there is no perturbation applied to the subjects. Instead, these works rely

on lower limb EMG and inverse dynamics to estimate stiffness. The current literature lacks experimentally obtained knee impedance values during stance phase as well as experimental validation of the aforementioned model based approaches. The knowledge of knee impedance during swing phase is also sparse, with only two studies existing and among those two studies, notably different time horizons for impedance estimation.

In this study, we estimate the impedance parameters of the human knee joint in both the stance and swing phases of walking, during several points of the gait cycle. We provide a succinct overview of the reconfiguration of an exoskeleton to optimize its utility for human system identification. Subsequently, we conduct a perturbation experiment involving 10 participants on a treadmill and estimate their knee joint impedance during walking. Following impedance estimation, we conduct a comprehensive analysis of the results by employing various statistical metrics. This analysis investigates multiple topics such as the influence of the exoskeleton on user gait, the model fit of estimated impedance parameters, and significant factors affecting impedance estimation. Finally, we contextualize these findings within existing literature and contemplate the implications of our results for the biomimetic control of wearable robots.

4.2 Methods

4.2.1 Exo Design

For this experiment, we utilized an exoskeleton with a QDD actuator as our perturbation device. The Modular Backdrivable Lower-limb Unloading Exoskeleton (MBLUE) has shown strong torque estimation abilities and low output impedance which is important for human system identification experiments [72]. However, the original version of this exoskeleton was not designed to perform perturbation experiments, so we

redesigned multiple aspects of the device to make it suitable for our research purposes. To minimize the effects of exoskeleton weight on user leg dynamics, we relocated the battery and microcontroller off the device, decreasing device weight (4B, Raspberry Pi Foundation, Cambridge, UK). We also implemented a waist mounted suspension system to counteract the device's weight and prevent sliding. Through pilot testing, we found that there was a discrepancy in motion between the exoskeleton's encoder and the human joint due to biological compliance. To ensure measurement of true joint displacement, we used an electrogoniometer (MLTS700, AD Instruments, Colorado Springs, CO) to measure joint motion. We removed the medial component of the exoskeleton to ensure correct placement of the goniometer across the subject's knee joint.

We found the removal of the medial side of the exoskeleton introduced torsional loading to the leg when perturbations were applied. This torsion created motion that was incorrectly identified by the goniometer as joint motion. To fix this, we changed the attachment points from the side of the leg to the front and back of the leg through the introduction of L brackets. These L brackets served to mitigate rotation by applying forces to the front and back of the leg, generating a pure torque around the knee in the sagittal plane. These brackets also incorporated adjustable slots that permitted the exoskeleton attachments points to be angled, allowing the device to conform to the user's anatomy. To ensure that subjects donning our exoskeleton had unfettered motion, we removed the original shoe suspension mechanism. We found that the shoe suspension adversely impacted ankle kinematics during walking and with the inclusion of our waist mounted suspension system there was no need for another suspension system. Removal of the shoe suspension also eliminated the need for specialized footwear, previously required for knee only version of MBLUE.

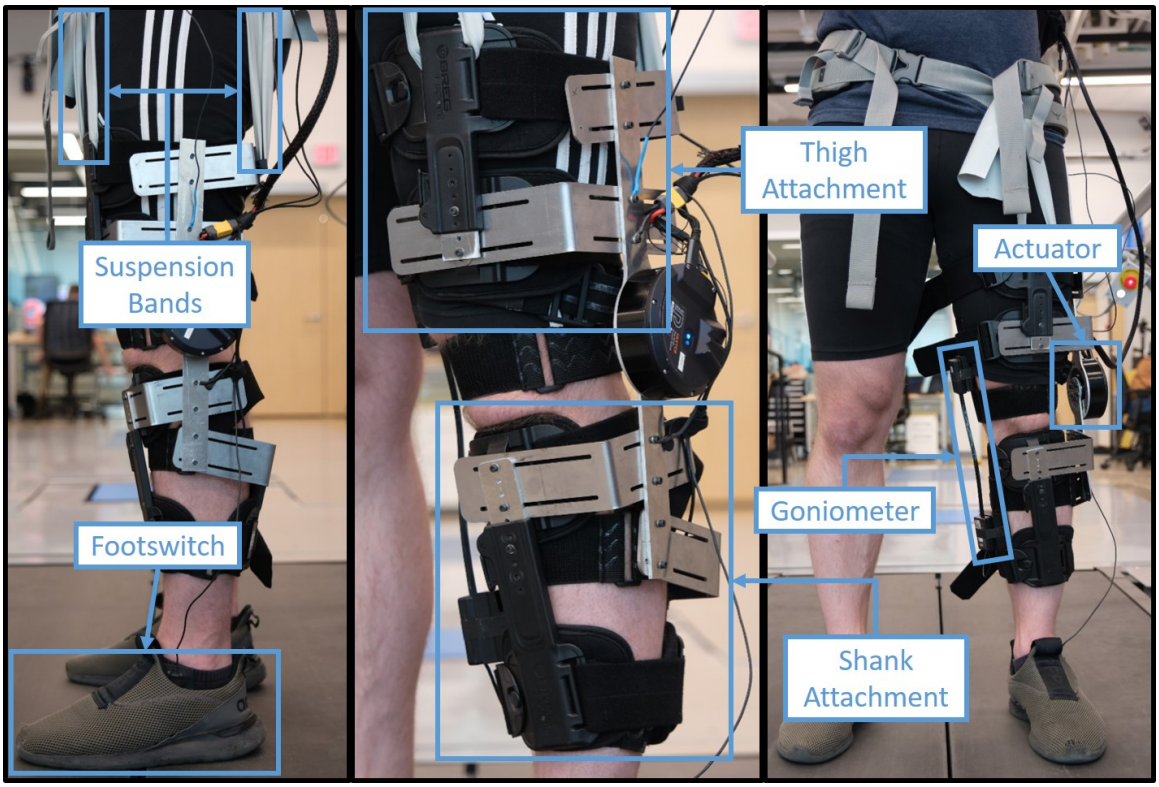

Figure 4.1: *Labeled figure of the exoskeleton utilized with human experimental participants*

4.2.2 Experimental Setup

We performed perturbation experiments with an exoskeleton on a diverse group of participants. Our study had N=10 able-bodied participants (4 female, mean age: 27.8 ±5.12 years, mean mass: 73.39 ±9.72 kg, mean height: 170.18 ±12.19 cm). Prior to data collection, subjects gave informed consent to a protocol approved by the University of Michigan Institutional Review Board (ID: HUM00154646). Each subject underwent three walking conditions, two of which occurred while wearing a knee exoskeleton; a non-exoskeleton walking condition (NWC), an exoskeleton walking condition with no perturbations (ENP), and an exoskeleton walking condition where perturbations were applied to the participant (EWP). The NWC condition was conducted to obtain a baseline for participant biomechanics without the exoskeleton. The ENP case was used to obtain a measure of the underlying mechanics displayed by

the subjects while wearing the perturbation device. Finally, the EWP condition was used to apply perturbations to participants for impedance estimation. All conditions occurred on a treadmill moving at a speed of 1.2 m/s. The NWC condition consisted of the subject walking without donning the exoskeleton for approximately 60 gait cycles. The ENP condition was also conducted for approximately 60 gait cycles. During the ENP condition, participants walked on the treadmill as the exoskeleton tracked a zero torque reference trajectory.

During the EWP condition, participants were perturbed at six time points within the gait cycle. During non-perturbation times, the exoskeleton minimized output impedance as participants walked on the treadmill. The six timing points where perturbation onset transpired were at 7%, 21.5%, 40.5%, 56%, 68.5%, and 81% of the participant's gait cycle. These timing points were in the middle of the loading response (LRE), mid-stance (MST), terminal stance (TST), pre-swing (PSW), initial swing (ISW), and mid-swing (MSW) phases of gait from [75]. Subject perturbations were applied in the direction of knee flexion. At each time point, 50 perturbations occurred. Every perturbation took the form of a 17 Nm torque hold and was applied for 250 ms. Perturbations were randomly applied to subjects in intervals of three to seven gait cycles. Torque perturbation information was determined offline with (4.1) where where the output torque, τ, is characterized by the gear ratio of the motor, g_r, the torque constant of the motor, k_t, the q-axis current drawn by the motor, I_q, the motor's coulomb friction, f_c, the motor's velocity, $\dot{\theta}$, the gear friction in the motor, f_g, the rotor inertia of the motor, J, and the motor's acceleration, $\ddot{\theta}$. All position and torque data were filtered in MATLAB (R2019b, Mathworks Inc., Natick, MA) using a fourth order butterworth filter with a cutoff frequency of 20 Hz:

$$\tau = g_r k_t I_q - (f_c + f_g|I_q|)\text{sign}(\dot{\theta}) - J\ddot{\theta}. \tag{4.1}$$

4.2.3 Human Impedance Estimation

To estimate impedance parameters, we performed regression on the experimentally obtained data after removing any underlying dynamics. For both the EWP and ENP cases, torque and position data from individual gait cycles were segmented based on heel strike data collected from a footswitch (LEMO, B&L Engineering, Santa Ana, CA). In the ENP case, the torque and position data from individual gait cycles were averaged to create a representative mean torque and position trajectory. For the EWP cases where perturbations were introduced, gait cycles were categorized based on perturbation onset timing. Each grouping of perturbed gait cycles was bootstrapped using the methods from [61]. The average torque and position data from the ENP case were subtracted from each bootstrapped EWP gait cycle group, removing the underlying dynamics of human walking and retaining solely the joint response to the perturbation. The isolated torque and position perturbations were then fed into a bounded least squares regression to estimate stiffness, K, damping, B, and inertial, J, impedance parameters. We normalized K and B by subject weight and reported the average value of all parameters, K, B, J, at each timing point.

4.2.4 Statistical Analysis

We employed several statistical techniques to analyze our experimental results. Variance Accounted For (VAF) was utilized to assess the how well the estimated impedance parameters fit to a second order linear model (4.2).

$$\tau = K\theta + B\dot{\theta} + J\ddot{\theta} \tag{4.2}$$

Additionally, a two-way Analysis of Variance (ANOVA) was conducted on a general linear model, with each model corresponding to an impedance parameter as the dependent variable as seen in (4.3). The linear model included the fixed independent

variable called timing point, tp, and the random independent variable called subject, $(1|subject)$. A Bonferroni correction was used for all post-hoc comparisons and the significance level for all tests was set to $\alpha = 0.05$.

$$(K, B, J) \sim 1 + tp + (1|subject) \tag{4.3}$$

The study also employed the use of Statistical Parametric Mapping (SPM) to assess the impact of wearing the exoskeleton on user biomechanics. SPM incorporates random field theory to compare spatiotemporal trajectories and determine if they are statically different [82]. In our case, we used SPM to perform a paired, two-tailed t-test on the mean position trajectories generated from the NWC and ENP cases. All 1D SPM analyses were implemented using the open-source 1D SPM code (v M.0.4.11, www.spm1d.org) in MATLAB. Significance was set at $\alpha = 0.05$.

To investigate the differences between knee quasi stiffness and our stiffness estimates, an unpaired t-test was performed on the two groups. The data to calculate quasi stiffness was taken from Winter's data and compared to impedance estimates made at the same points in the gait cycle [83]. A percent difference calculation was performed to further elucidate the differences between quasi-stiffness and impedance.

4.3 Results

4.3.1 Effects of Exoskeleton Hardware on Walking Gait

Subject gait was not affected by donning the exoskeleton during the experiment. Figure 4.2 shows the average position and torque trajectory of a representative subject during the ENP condition. SPM analysis showed that the NWC and ENP walking trials were not statistically significantly different, accepting the null hypothesis, as the t-statistic trajectory always fell within t-value threshold of $t = \pm 4.299$ (Figure

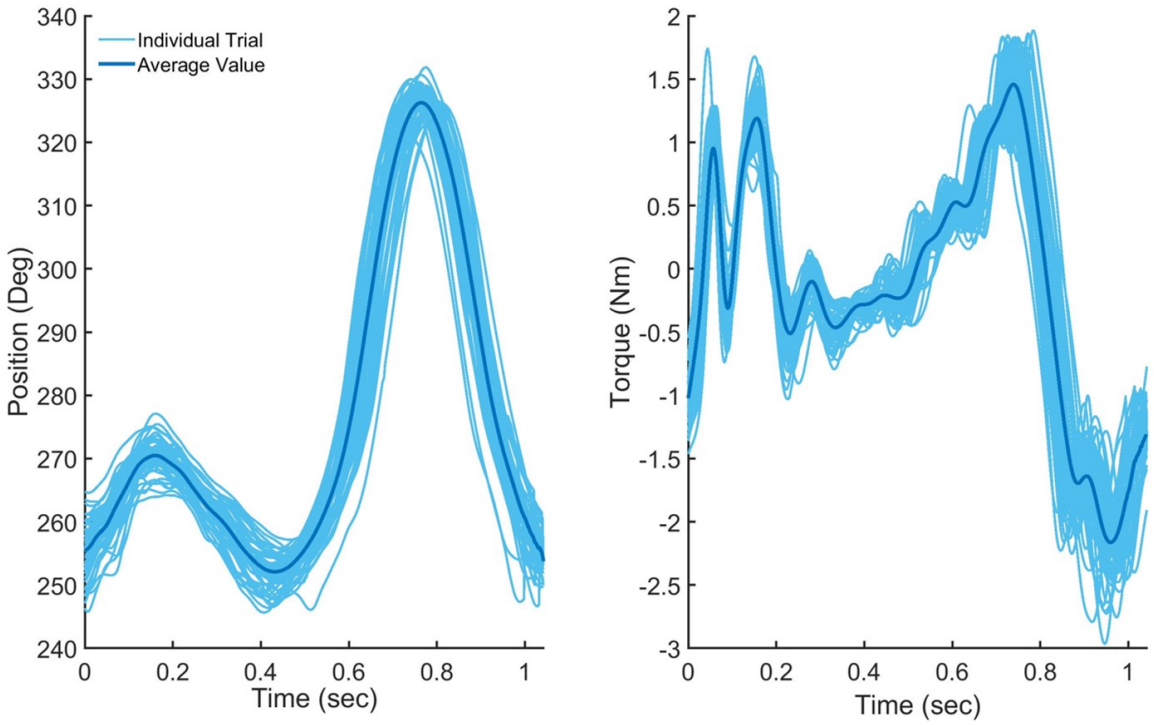

Figure 4.2: *Individual and mean position and torque trajectories of subject 9 during the ENP case.*

4.3).

4.3.2 Knee Impedance throughout Gait Cycle

4.3.2.1 Population Averages

Stiffness values showed the most variation amongst the three types of impedance estimates with damping and inertia values remaining more consistent over the length of the gait cycle. Individual subject and average stiffness, damping, and inertia values are in tables 4.1,4.2, and 4.3 respectively. Average stiffness values ranged from 2.13 to 0.31 Nm/rad/kg, showing the highest stiffness value during the loading response phase of gait. Average damping showed linearly increasing behavior during stance phase and ranged from 0.053 to 0.030 Nms/rad/kg. Average inertia demonstrated oscillatory constant between most timing points, ranging from 0.040 to 0.023 kgm^2. The average VAF across all subjects and timing points was 90.62 $\pm$ 4.32%. A table

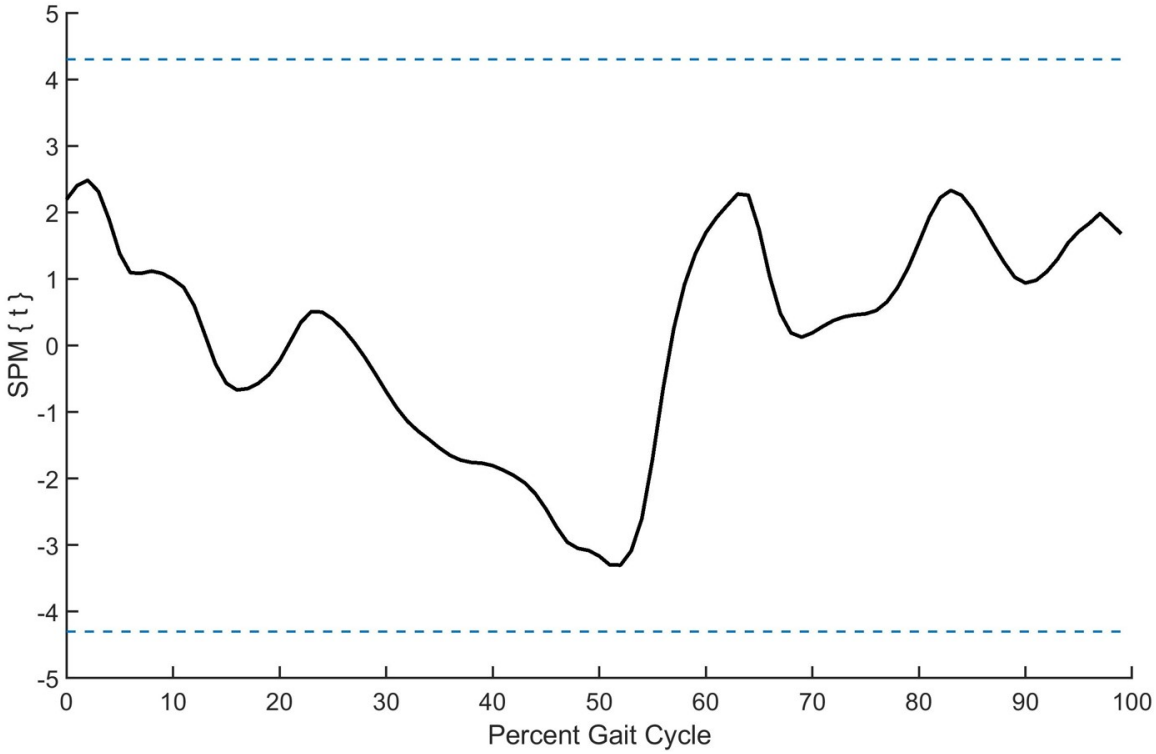

Figure 4.3: *The SPM test statistic trajectory indicating if the mean position trajectories from the NWC and ENP cases are statistically significantly different. The dashed blue line representing the t-value threshold as determined by an SPM two-tailed t-test. The null hypothesis is rejected at* $\alpha = 0.05$ *if the test statistic trajectory (thick black line) crosses the threshold*

Table 4.1: *Table of individual and average subject stiffness. Stiffness has units of* $Nm/rad/kg$.

Timing Points	Subjects										
	S1	S2	S3	S4	S5	S6	S7	S8	S9	S10	Avg
LRE	1.88	1.76	4.23	1.72	2.12e-14	1.58	0.54	6.59	1.78	1.23	2.13
MST	0.76	0.60	0.17	0.09	0.21	0.24	0.71	1.79	0.78	0.82	0.62
TST	1.52	0.72	1.31	2.03	1.00	1.08e-4	0.82	2.26	0.60	1.21	1.15
PSW	1.91	1.19	0.40	1.36	0.97	0.97	1.14	2.71	0.97	0.02	1.16
ISW	0.75	0.17	0.26	0.30	0.0082	0.048	0.13	4.88e-12	0.78	0.70	0.31
MSW	0.68	0.22	2.04e-5	0.0042	0.62	0.43	0.51	0.54	0.69	0.11	0.38

Table 4.2: *Table of individual and average subject damping. Damping has units of* $Nms/rad/kg$.

Timing Points	Subjects										
	S1	S2	S3	S4	S5	S6	S7	S8	S9	S10	Avg
LRE	0.024	0.074	1.07e-11	0.073	0.073	0.047	0.064	1.68e-11	0.023	0.0082	0.039
MST	0.055	0.046	0.076	0.060	0.057	0.040	0.043	3.65e-12	0.031	0.011	0.042
TST	0.051	0.060	0.058	0.081	0.028	0.096	0.074	0.019	0.066	4.30e-4	0.053
PSW	0.011	0.038	0.040	0.042	0.026	0.014	0.028	0.0068	0.018	0.072	0.030
ISW	0.031	0.063	0.053	0.053	0.056	0.032	0.020	0.028	0.020	0.026	0.038
MSW	0.035	0.042	0.043	0.049	0.015	0.015	0.014	0.025	0.014	0.034	0.029

of all VAFs can be seen in table 4.4.

4.3.2.2 Factors Influencing Knee Impedance

Timing point and subject were found to be important factors that influenced impedance estimates. The ANOVA results for all linear models found timing point and subject to be significant ($p < 0.001$). Analyzing the stiffness linear model showed timing points 1 and 2 to be significantly different from all other timing points. Timing points 3 and 4 were found to be similar to each other and timing points 5 and 6 were found

Table 4.3: *Table of individual and average subject inertia. Inertia has units of kgm^2 and is the combined inertia of the device and joint.*

Timing Points	Subjects										
	S1	S2	S3	S4	S5	S6	S7	S8	S9	S10	Avg
LRE	0.018	0.014	0.0015	0.011	0.068	0.051	0.047	0.030	0.021	0.0080	0.027
MST	0.0033	0.010	0.027	0.14	0.031	0.065	0.033	0.047	0.0055	0.0026	0.036
TST	1.99e-10	0.030	0.065	0.14	0.029	0.060	0.0085	0.017	0.0081	0.0081	0.024
PSW	0.024	0.030	0.070	0.039	0.051	0.050	0.022	0.052	0.032	0.032	0.040
ISW	0.019	0.032	0.030	0.023	0.032	0.043	0.069	0.030	0.018	0.038	0.033
MSW	5.02e-11	0.011	0.024	0.016	0.053	0.029	0.040	0.030	0.013	0.011	0.023

Table 4.4: *Table of individual and average subject VAF's. All entries are percentages.*

Timing Points	Subjects										
	S1	S2	S3	S4	S5	S6	S7	S8	S9	S10	Avg
LRE	97.51	97.82	93.68	92.93	45.20	75.79	94.38	84.48	96.95	99.65	87.84
MST	96.75	98.28	93.46	98.96	92.48	94.50	90.76	86.50	98.22	99.30	94.92
TST	96.56	96.68	98.62	96.78	93.18	93.02	99.24	96.02	99.24	99.83	96.92
PSW	93.54	98.37	64.90	88.72	91.20	94.02	94.38	64.04	95.19	93.37	87.77
ISW	91.36	98.79	78.31	78.45	80.97	91.69	66.85	96.03	93.30	86.82	86.26
MSW	85.41	97.03	80.08	92.99	87.95	91.83	90.76	84.19	94.07	95.90	90.02

to be similar to each other. The damping linear model showed timing point 3 to be different than all other points. Timing points 4 & 6 were found to be similar to each other. The damping values at timing points 1, 2, and 5 were found to be similar. Inertia estimates showed more complex relationships between timing points. Timing point 4 was found to be different from all other timing points. Timing points 2 and 5 were not significantly different. Interestingly timing point 3 was similar to points 1 and 6 but timing points 1& 6 were not similar.

4.3.2.3 Comparison to Quasi Stiffness

Percent different calculations made quasi stiffness appear notably different from stiffness but further statistical analysis showed the results to be similar. Quasi-stiffness was not found to not be statistically different from stiffness in this study ($p = 0.3374$).

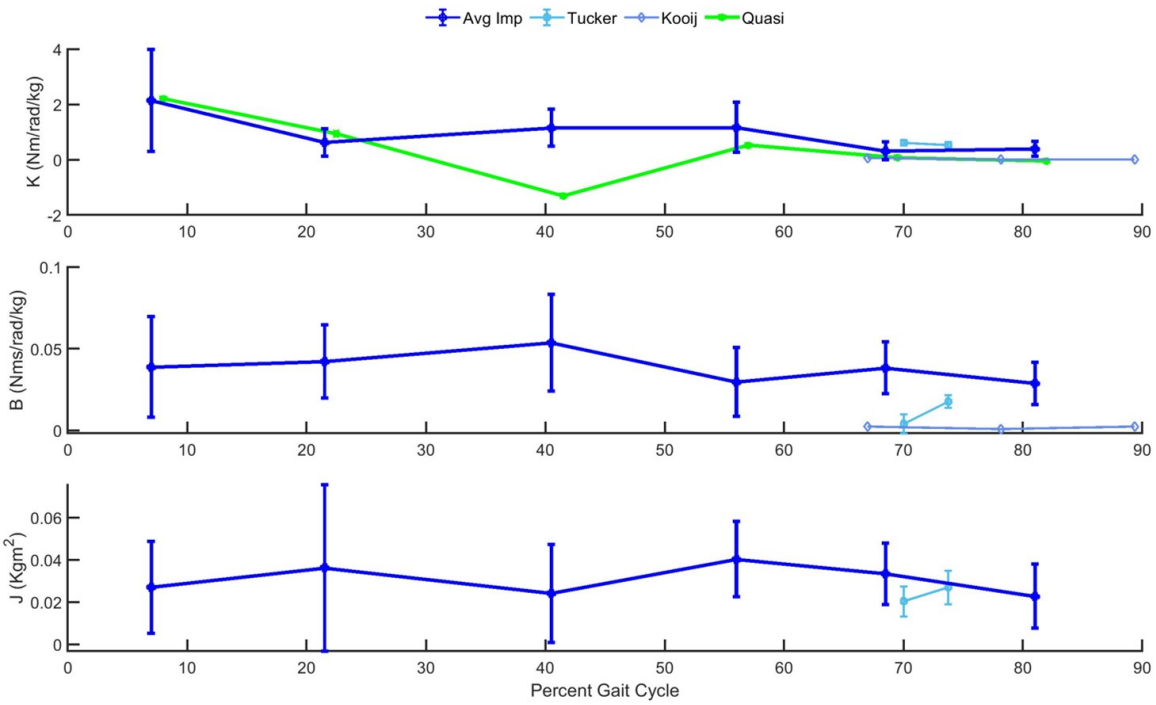

Figure 4.4: *Average knee impedance estimates from all subjects during walking. Subjects were perturbed at six phases of the gait cycle and knee joint impedance was estimated at these points. Top shows stiffness normalized by mass, middle shows damping normalized by mass, and bottom shows inertia. Quasi stiffness as well as other experimental impedance results are shown as well. Quasi stiffness data is offset from stiffness estimates for clarity.*

A visual comparison of quasi stiffness and stiffness can be made from figure 4.4. The percent difference of quasi-stiffness with respect to stiffness was 3.44%, 51.85%, -214.24%, -54.61%, -77.72%, -112.67% for 7%, 21.5%, 40.5%, 56%, 68.5%, and 81% of the participant's gait cycle respectively.

4.4 Discussion

This study investigated knee impedance modulation throughout the gait cycle by using an exoskeleton to perturb and collect data on multiple subjects during a walking experiment. We applied a 17 Nm torque perturbation to our participants at 6 unique points of their gait cycle. Then, we extracted the position and torque information from this perturbation and used it in a least squares regression to estimate the stiffness,

damping, and inertia properties of the subjects during gait. A myriad of statistical analyses were performed on the data collected and we found that our device does not have a statistically significant effect on the knee biomechanics of those who wear it. We also found that the point of the gait cycle where we perturb people as well as the individual who is being perturbed has a significant effect on the estimate of impedance. Our last major finding was that the quasi stiffness values of the knee closely match our stiffness estimates for most of the gait cycle.

We found that our stiffness and inertia estimates matched results from other knee perturbation studies closely but our damping estimates did not. All of our damping estimates were higher than the corresponding literature and there are a few possibilities as to why this is so. In the case of Kooij's work, we believe the discrepancy in magnitude is a result of different time windows for analysis. Kooij uses a much longer analysis window at 275 ms than ours which is 100 ms. This much longer time window permits the torque generated from reflexes to be much larger, and therefore have a larger effect on the impedance estimates at the joint [79]. The difference in magnitude from Tucker's work may be the result of unaccounted for dynamics in their model. While Tucker's work uses a 100 ms time analysis window like this work, their average VAF across all timing points and subjects was $\sim$72%. This VAF is low for human impedance studies and may imply that their model parameters were not strong predictors of data variance. Our VAF across all subjects and timing points was $\sim$91%, showing a much stronger model fit. We believe the difference in model fits can explain the magnitude discrepancies between the two sets of damping estimates.

The model based estimates of impedance followed similar trends as our data but had notably different stiffness magnitudes (A.1). During stance phase, we found that the trends of these modeling approaches follow the trends of our data with a high stiffness during early stance then decrease in stiffness during mid stance and concluding with

an increase in stiffness towards the end of stance. In swing, we saw an agreement in the trends of the data, with a notable decrease in stiffness after toe off. However we found the magnitude of stiffness estimates from the model based approaches to be very different than ours in both stance and swing. The sections of gait where we saw the largest difference in estimates were in early stance phase and during swing. We did see similar magnitudes for estimates during mid stance. Sartori's values matched ours well in terminal stance but Pfeifer's estimates were higher than our estimates. During swing phase, we see Pfeifer's estimates continuing to be larger than ours by a factor of approximately two or three. We believe these differences may stem from a lack of perturbations being used in the model based studies. Previous work has shown that applying perturbations is crucial to accurately estimating impedance. Without perturbations, the identification of the closed loop system will be heavily skewed by the characteristics of the input's noise [67]. Future studies using both model based and experimental approaches on the same subjects should be done to further explore the discrepancies between model based and experimental results.

Our knee impedance estimates demonstrated similar behavior as estimates of ankle impedance with respect to quasi stiffness but the trends of the knee data are less clear than the ankle. In stance at the both ankle and knee, we found that joint quasi stiffness closely mimicked stiffness excluding for the toe off portion of gait. Literature has shown quasi stiffness and impedance to be distinct entities, however this is the second lower limb joint where this behavior has been reported [61, 69, 84]. The similarities between the two quantities may be highlighting that while quasi-stiffness and impedance have notable differences during volitional movements, during periods where intrinsic joint properties dominate, quasi stiffness may be a good approximation for impedance behavior. During swing phase, we found that the trends of low stiffness and damping values mimic what is seen in the ankle literature [68]. However, during mid to late stance the clear inverse relationship between stiffness and damping seen

at the ankle is not mirrored at the knee [61, 69]. This could be a result of the knee and ankle serving different purposes for gait. The ankle stores large amounts energy and generate power during this during gait while the knee serves a stabilization and energy exchange role [85].

These results have important implications on robotic biomimetic control, particularly as it applies to the control of prosthetic devices. Multiple papers have used biologically inspired control laws on wearable robotic devices, with prosthetic knees being a commonly utilized medium [9, 64, 86, 10, 87, 88]. In our analysis, we saw that timing point and subject had significant effects on impedance estimates. We take these results to demonstrate two points: first, that constant impedance control is not sufficient for true biomimetic control, and second, that impedance controllers should be tailored to the individual using the device. Studies have shown that people report improved comfort and display better performance with personalized controllers [89, 90, 91, 92, 93, 94]. Our results in combination with the literature, compel us to recommend using individualized impedance controllers for best results. An example of this could be using the results of this work as an initial guess for a biomimetic impedance controller and then using a personalization method, such as human in the loop (HILO) optimization, to fine tune a control law for a prosthetic device.

4.4.1 Limitations

In our analysis, certain assumptions were made to establish a framework for our study. We considered the knee joint to be a second-order system and assumed linearity and time-invariance (LTI) during our analysis window. Previous literature has shown that representing human joints as second order, linear time invariant systems can account for more than 97% of model variance, providing us confidence in our assumptions [67].

We experienced practical limitations during our study that prevented us from capturing all eight phases of the gait cycle. We found that it was difficult to obtain impedance estimates during the initial contact (ICO) and terminal swing (TSW) phases of gait. ICO constitutes only 2% of the gait cycle which meant that the perturbation often extended into the LRE phase. One way to fix this issue may be to use a shorter analysis window. However, a potential issue with using a smaller analysis window is the potential latency between perturbation application and measured joint displacement. This issue can arise due to sub-optimal exoskeleton interfacing or human soft tissue. Issues with data capture during TSW arose because the length of the TSW phase showed high variability between gait cycles, sometimes being so brief that perturbations encroached into the ICO phase. One potential solution to this issue could be initiating perturbations earlier in the gait phase, at times such as 10% instead of 50%. The absence of data from these gait phases impedes our ability to gain insights into the transition from swing to stance, and future studies should look to remedy these issues.

Another limitation of this work is that it does not distinguish between the reflexive and intrinsic components of joint impedance. While we believe that the impedance results shown in this work are primarily reflective of the intrinsic behavior of the knee joint, we acknowledge that reflex force generation can start at 40 ms, with max reflex contributions occurring 60 ms after the 40 ms point [79, 95]. However, research shows that reflex contributions are lower during locomotion [96, 29]. With our use of a 100 ms analysis window, we believe that the effect of the reflex contribution is less than that of the response that is a result of the underlying knee musculature.

CHAPTER V

Conclusions and Future Work

5.1 Summary of Work

In chapter two, I validated the system identification capabilities of a torque-controllable knee exoskeleton and proposed a perturbation paradigm for the identification of the impedance known mass-spring systems with the intention of extending this work to estimate the mechanical impedance of the human knee during locomotion. The proposed methods yielded stiffness estimate errors of ∼2-2.5% damping values centered around zero and dominated by noise, and inertia estimate errors ranging from ∼13-15%, which can likely be improved by other numerical methods. I also learned that the analysis techniques tended to underestimate of impedance parameters and that experimental factors such as the frequency of the underlying trajectory and type of perturbation applied by the exoskeleton have an effect on the efficacy of the device's results. From the conclusions drawn from the data, I was confident that these methods could be utilized to accurately characterize human joint mechanical impedance during locomotion in future studies.

In chapter three, I characterized a perturbation system that used a highly backdrivable quasi-direct-drive actuator and a carefully calibrated actuator torque model. Bench top validation with known mechanical impedance human-substitutes, con-

firmed the viability of this system as an impedance measurement tool. Identification of the human substitute system under static conditions yielded an error of under 1% while identification under dynamic conditions produced error of ∼5%. A pilot study with two subjects utilizing a custom knee-exoskeleton apparatus confirmed the feasibility of this system for human walking experiments. This pilot study produced the first experimentally estimated knee impedance values during the stance phase of gait. Additionally, this study also produced impedance estimates during portions of the swing phase of gait that have not been reported in the literature.

In chapter four, I investigated knee impedance modulation throughout the gait cycle by using an exoskeleton to perturb and collect data on multiple subjects during a walking experiment. I applied a 17 Nm torque perturbation to the participants at six unique points of their gait cycle. I then used the position and torque information gleaned from this experiment to perform a least squares regression. This regression estimated the stiffness, damping, and inertia properties of the subjects during gait. A myriad of statistical analyses were performed on the data collected producing three major takeaways, First, I found that our device does not have a statistically significant effect on the knee biomechanics of those who wear it. Second, the point of the gait cycle where we perturb people as well as the individual who is being perturbed has a significant effect on the estimate of impedance. Finally, the quasi stiffness values of the knee closely match our impedance estimates of the knee for most of the gait cycle.

5.2 Contributions

This work fills gaps found in the academic literature with research that has real world applications. The work in this thesis validated the methods for impedance estimation used in [2] using different inputs and a different system. Through the validation

of these methods, I demonstrated improvements in the ability to estimate stiffness by decreasing average stiffness estimation error from 5% to under 3%. By using these methods on a different platform with different inputs, I also have demonstrated the robustness of these methods for impedance estimation. I also produced a novel configuration of a previously constructed exoskeleton, through mechanical redesign, providing the first account of using this device for human system identification. I have made significant contributions to the knee impedance literature, by producing the first experimentally estimated values of knee impedance during the stance phase of walking. I also produced estimates of impedance at points during the swing phase of gait that have never been explored.

5.3 Future Work

A key objective of this work is to provide basic science information to further robotic control and I would recommend creating a collection of impedance information under various conditions, speeds, and environments to support that effort. One condition that should be included in this collection of data is walking on angled terrains. Gathering impedance data during walking on slopes of various angles can provide more data to human based impedance controllers, increasing their robustness [97, 98, 99]. Another is walking in non laboratory settings. Walking in non laboratory controlled situations has more variation than walking in treadmill situations due to a non constant walking speed, amongst other factors [100]. If the timing based approach used in this work may be too susceptible to the error that non laboratory walking produces, using alternate methods for gait cycle tracking, like those in Best *et al.*, should produce gait heel strike estimates that are more robust to non laboratory experimental variance [101].

The completion of this work has made it clear that it takes considerable time and

effort to produce quality experimental methods. I believe that refining model based approaches with experimental data would be useful for precipitously decreasing the time required to acquire impedance estimates. Chapter four discussed how model based approaches typically over estimated knee impedance values. Conducting future experiments that can simultaneously collect the data needed for model based estimation as well as experimental impedance estimation will be paramount to this end. Running these joint experiments is so important because it will produce baseline estimates for the model based approaches to compare themselves to. I believe refining these model based approaches will permit impedance experiments to scale better, not requiring the large amounts of time necessary to design a perturbation device and experiment with participants.

These data produced here now permits the use of a unified biomimetic impedance controller for ankle and knee prosthesis. Typically people have used data fitting methods on human data to create impedance control laws for prostheses [9, 64, 86, 10, 87, 88, 102]. With this data, people can now test biologically accurate impedance control laws and investigate what effects this control strategy has on prosthesis users. Measure that may be particularly useful to investigate are gait biomechanics, stability, user preference, and external disturbance rejection. Exploring how biologically accurate impedance control compares to data fitted impedance control laws with respect to these metrics can demonstrate if there is a need for experimental impedance studies.

Knowledge of knee impedance modulation may also provide utility in the rehabilitation space. Work from Shorter showed that impedance changes with age and after neurological disorder [103]. Using a combination of these data produced here and the impedance information in the literature, I believe we can use impedance as a metric to help inform rehabilitative practices. Some examples of this could include using

exoskeletons with survivors of stroke to render age appropriate impedances at the joint of interest, assessing impedance trajectories as people go through rehabilitative treatments such as physical therapy.

APPENDIX

APPENDIX A

Knee Stiffness Comparisons

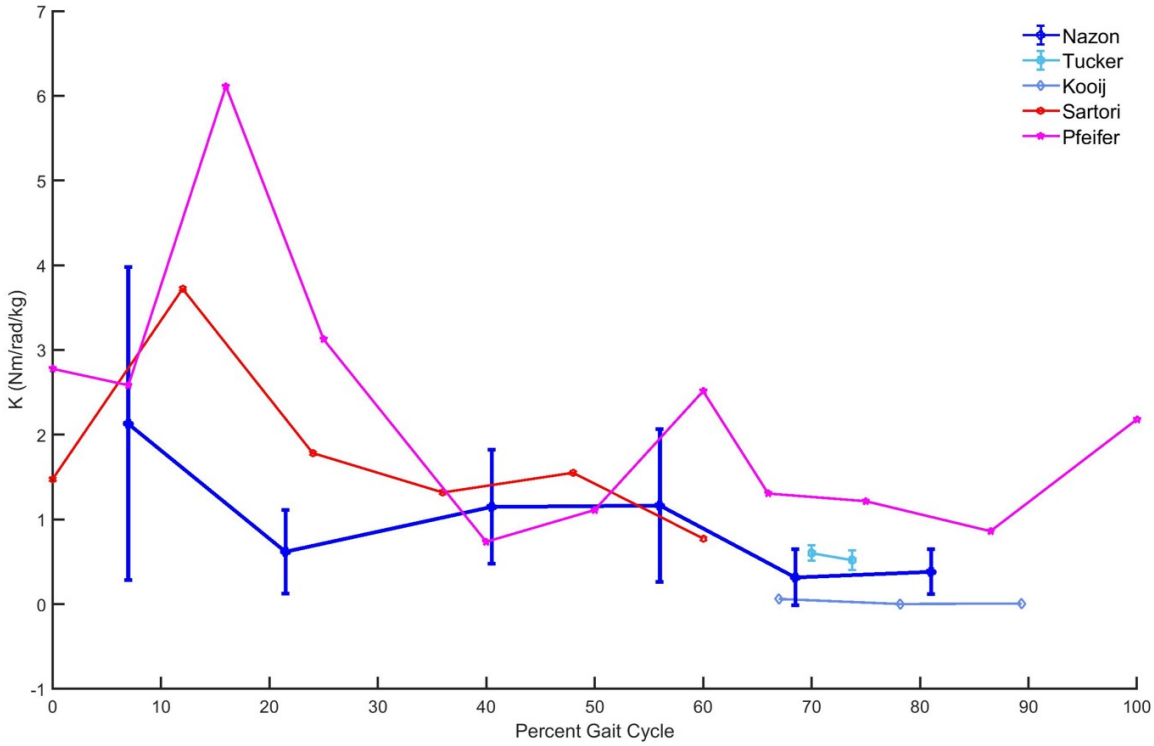

Figure A.1: *Knee stiffness estimates from this work with relation to other literature. Tucker and Kooij reference studies that utilized experimental perturbation methods. Sartori and Pfeifer reference works that used EMG model based approaches to estimate stiffness.*

BIBLIOGRAPHY

BIBLIOGRAPHY

[1] Robert E. Kearney and Ian W. Hunter. System Identification of Human Joint Impedance. *Journal of the American Society for Information Science*, 1990.

[2] Elliott J. Rouse, Levi J. Hargrove, Eric J. Perreault, and Todd A. Kuiken. Estimation of human ankle impedance during the stance phase of walking. *IEEE Transactions on Neural Systems and Rehabilitation Engineering*, 22(4):870–878, 2014.

[3] Arthur D Kuo and J Maxwell Donelan. Dynamic principles of gait and their clinical implications. *Physical Therapy*, 90(2):157–174, 2010.

[4] Etienne Burdet, Rieko Osu, David W. Franklin, Theodore E. Milner, and Mitsuo Kawato. The central nervous system stabilizes unstable dynamics by learning optimal impedance. *Nature*, 414(6862):446–449, 2001.

[5] Xiao Hu, Daniel Ludvig, Wendy M. Murray, and Eric J. Perreault. Using Feedback Control to Reduce Limb Impedance during Forceful Contractions. *Scientific Reports*, 7(1):1–13, 2017.

[6] Alexander M Wind and Elliott J Rouse. Neuromotor Regulation of Ankle Stiffness is Comparable to Regulation of Joint Position and Torque at Moderate Levels. *Scientific Reports*, 10(10383):1–9, 2020.

[7] Neville Hogan. Impedance control: An approach to manipulation: Part ii—implementation. 1985.

[8] Mariah W Whitmore, Levi J Hargrove, and Eric J Perreault. Gait characteristics when walking on different slippery walkways. *IEEE Transactions on Biomedical Engineering*, 63(1):228–239, 2015.

[9] Frank Sup, Amit Bohara, and Michael Goldfarb. Design and control of a powered transfemoral prosthesis. *The International journal of robotics research*, 27(2):263–273, 2008.

[10] Michael R Tucker, Jeremy Olivier, Anna Pagel, Hannes Bleuler, Mohamed Bouri, Olivier Lambercy, José del R Millán, Robert Riener, Heike Vallery, and Roger Gassert. Control strategies for active lower extremity prosthetics and orthotics: a review. *Journal of neuroengineering and rehabilitation*, 12(1):1–30, 2015.

[11] Bram Koopman, Edwin HF van Asseldonk, and Herman van der Kooij. Estimation of human hip and knee multi-joint dynamics using the lopes gait trainer. *IEEE transactions on robotics*, 32(4):920–932, 2016.

[12] M. K. Shepherd and E. J. Rouse. The VSPA Foot: A Quasi-Passive Ankle-Foot Prosthesis With Continuously Variable Stiffness. *IEEE Transactions on Neural Systems and Rehabilitation Engineering*, 25(12):2375–2386, 2017.

[13] E. M. Glanzer and P. G. Adamczyk. Design and validation of a semi-active variable stiffness foot prosthesis. *IEEE Transactions on Neural Systems and Rehabilitation Engineering*, 26(12):2351–2359, 2018.

[14] Alejandro F Azocar, Luke M Mooney, Jean-François Duval, Ann M Simon, Levi J Hargrove, and Elliott J Rouse. Design and clinical implementation of an open-source bionic leg. *Nature biomedical engineering*, 4(10):941–953, 2020.

[15] Neville Hogan. Impedance control: An approach to manipulation. In *1984 American control conference*, pages 304–313. IEEE, 1984.

[16] Herman Van der Kooij, Simone S Fricke, Ronald C van't Veld, Ander Vallinas Prieto, Arvid QL Keemink, Alfred C Schouten, and Edwin HF Van Asseldonk. Identification of hip and knee joint impedance during the swing phase of walking. *IEEE transactions on neural systems and rehabilitation engineering*, 30:1203–1212, 2022.

[17] Elliott Jay Rouse. Estimation of human ankle impedance during walking for powered prosthesis control, 2012.

[18] Hsien Yung Huang, Arash Arami, Ildar Farkhatdinov, Domenico Formica, and Etienne Burdet. The influence of posture, applied force and perturbation direction on hip joint viscoelasticity. *IEEE Transactions on Neural Systems and Rehabilitation Engineering*, 28(5):1138–1145, 2020.

[19] R Crowninshield, MH Pope, R Johnson, and R Miller. The impedance of the human knee. *Journal of Biomechanics*, 9(8):529–535, 1976.

[20] Li-Qun Zhang, Gordon Nuber, Jesse Butler, Mark Bowen, and William Z Rymer. In vivo human knee joint dynamic properties as functions of muscle contraction and joint position. *Journal of biomechanics*, 31(1):71–76, 1997.

[21] Changfeng Tai and Charles J. Robinson. Knee elasticity influenced by joint angle and perturbation intensity. *IEEE transactions on rehabilitation engineering : a publication of the IEEE Engineering in Medicine and Biology Society*, 7 1:111–5, 1999.

[22] Changfeng Tai and C. Robinson. Variation of human knee stiffness with angular perturbation intensity. *Proceedings of 17th International Conference of the Engineering in Medicine and Biology Society*, 2:1317–1318 vol.2, 1995.

[23] Hyunglae Lee, Patrick Ho, Mohammad Rastgaar, Hermano Igo Krebs, and Neville Hogan. Multivariable static ankle mechanical impedance with active muscles. *IEEE Transactions on Neural Systems and Rehabilitation Engineering*, 22(1):44–52, 2013.

[24] Ian D Loram and Martin Lakie. Direct measurement of human ankle stiffness during quiet standing: the intrinsic mechanical stiffness is insufficient for stability. *The journal of physiology*, 545(3):1041–1053, 2002.

[25] Anindo Roy, Hermano I Krebs, Christopher T Bever, Larry W Forrester, Richard F Macko, and Neville Hogan. Measurement of passive ankle stiffness in subjects with chronic hemiparesis using a novel ankle robot. *Journal of neurophysiology*, 105(5):2132–2149, 2011.

[26] Guilherme A Ribeiro, Lauren N Knop, and Mo Rastgaar. The 2-dof mechanical impedance of the human ankle during poses of the stance phase. In *Powered Prostheses*, pages 23–39. Elsevier, 2020.

[27] Gerald L Gottlieb and Gyan C Agarwal. Dependence of human ankle compliance on joint angle. *Journal of Biomechanics*, 11(4):177–181, 1978.

[28] Arash Arami, Edwin van Asseldonk, Herman van der Kooij, and Etienne Burdet. A clustering-based approach to identify joint impedance during walking. *IEEE Transactions on Neural Systems and Rehabilitation Engineering*, 28(8):1808–1816, 2020.

[29] Daniel Ludvig, Maciej Plocharski, Piotr Plocharski, and Eric J Perreault. Mechanisms contributing to reduced knee stiffness during movement. *Experimental brain research*, 235(10):2959–2970, 2017.

[30] Michael R Tucker. Development of a tool and a method for estimating knee impedance during gait. 2016.

[31] Hyunglae Lee, Elliott J Rouse, and Hermano Igo Krebs. Summary of human ankle mechanical impedance during walking. *IEEE Journal of Translational Engineering in Health and Medicine*, 4:1–7, 2016.

[32] Amanda L. Shorter and Elliott J. Rouse. Mechanical Impedance of the Ankle during the Terminal Stance Phase of Walking. *IEEE Transactions on Neural Systems and Rehabilitation Engineering*, 26(1):135–143, 2018.

[33] Kristen L Jakubowski, Daniel Ludvig, Daniel Bujnowski, Sabrina SM Lee, and Eric J Perreault. Simultaneous quantification of ankle, muscle, and tendon impedance in humans. *IEEE Transactions on Biomedical Engineering*, 69(12):3657–3666, 2022.

[34] Elliott J Rouse, Levi J Hargrove, Eric J Perreault, Michael A Peshkin, and Todd A Kuiken. Development of a mechatronic platform and validation of methods for estimating ankle stiffness during the stance phase of walking. *Journal of biomechanical engineering*, 135(8), 2013.

[35] Evandro M Ficanha, Guilherme A Ribeiro, Lauren Knop, and Mo Rastgaar. Time-varying impedance of the human ankle in the sagittal and frontal planes during straight walk and turning steps. In *2017 International Conference on Rehabilitation Robotics (ICORR)*, pages 1413–1418. IEEE, 2017.

[36] Varun Nalam and Hyunglae Lee. Design and validation of a multi-axis robotic platform for the characterization of ankle neuromechanics. In *2017 IEEE International Conference on Robotics and Automation (ICRA)*, pages 511–516. IEEE, 2017.

[37] Joshua B. Russell, Connor M. Phillips, Matthew R. Auer, Vu Phan, Kwanghee Jo, Omik Save, Varun Nalam, and Hyunglae Lee. Introduction to a twin dual-axis robotic platform for studies of lower limb biomechanics. *IEEE Journal of Translational Engineering in Health and Medicine*, 11:282–290, 2023.

[38] Hsien Yung Huang, Ildar Farkhatdinov, Arash Arami, Mohamed Bouri, and Etienne Burdet. Cable-driven robotic interface for lower limb neuromechanics identification. *IEEE Transactions on Biomedical Engineering*, 2020.

[39] Hyunglae Lee and Neville Hogan. Time-varying ankle mechanical impedance during human locomotion. *IEEE Transactions on Neural Systems and Rehabilitation Engineering*, 23(5):755–764, 2015.

[40] R. R. Neptune, F. E. Zajac, and S. A. Kautz. Muscle force redistributes segmental power for body progression during walking. *Gait and Posture*, 19(2):194–205, 2004.

[41] D. A. Winter. Energy generation and absorption at the ankle and knee during fast, natural, and slow cadences. *Clinical Orthopaedics and Related Research*, No. 175:147–154, 1983.

[42] Li Qun Zhang, Gordon Nuber, Jesse Butler, Mark Bowen, and William Z. Rymer. In vivo human knee joint dynamic properties as functions of muscle contraction and joint position. *Journal of Biomechanics*, 31(1):71–76, 1997.

[43] D. J. Bennett, J. M. Hollerbach, Y. Xu, and I. W. Hunter. Time-varying stiffness of human elbow joint during cyclic voluntary movement. *Experimental Brain Research*, 88(2):433–442, 1992.

[44] Florin Popescu, Joseph M. Hidler, and W. Zev Rymer. Elbow impedance during goal-directed movements. *Experimental Brain Research*, 152(1):17–28, 2003.

[45] Daniel Ludvig, Maciej Plocharski, Piotr Plocharski, and Eric J. Perreault. Mechanisms contributing to reduced knee stiffness during movement. *Experimental Brain Research*, 235(10):2959–2970, 2017.

[46] Serge Pfeifer, Heike Vallery, Michael Hardegger, Robert Riener, and Eric J. Perreault. Model-based estimation of knee stiffness. *IEEE Transactions on Biomedical Engineering*, 59(9):2604–2612, 2012.

[47] Serge Pfeifer, Robert Riener, and Heike Vallery. Knee stiffness estimation in physiological gait. *2014 36th Annual International Conference of the IEEE Engineering in Medicine and Biology Society, EMBC 2014*, (vm):1607–1610, 2014.

[48] Massimo Sartori, Marco Maculan, Claudio Pizzolato, Monica Reggiani, and Dario Farina. Modeling and simulating the neuromuscular mechanisms regulating ankle and knee joint stiffness during human locomotion. *Journal of neurophysiology*, 114(4):2509–2527, 2015.

[49] Kamran Shamaei, Gregory S. Sawicki, and Aaron M. Dollar. Estimation of Quasi-Stiffness of the Human Knee in the Stance Phase of Walking. *PLoS ONE*, 8(3), 2013.

[50] Elliott J. Rouse, Robert D. Gregg, Levi J. Hargrove, and Jonathon W. Sensinger. The difference between stiffness and quasi-stiffness in the context of biomechanical modeling. *IEEE Transactions on Biomedical Engineering*, 60(2):562–568, 2013.

[51] Mehmet Temel, Katherine S. Rudolph, and Sunil K. Agrawal. Gait recovery in healthy subjects: Perturbations to the knee motion with a Smart Knee Brace. *IEEE/ASME International Conference on Advanced Intelligent Mechatronics, AIM*, pages 527–532, 2010.

[52] James S. Sulzer, Ronald A. Roiz, Michael A. Peshkin, and James L. Patton. A highly backdrivable, lightweight knee actuator for investigating gait in stroke. *IEEE Transactions on Robotics*, 25(3):539–548, 2009.

[53] Jacob Buus Andersen and Thomas Sinkjær. Mobile Ankle and Knee Perturbator. *IEEE Transactions of Biomedical Engineering*, 50(10):1208–1211, 2003.

[54] Michael R. Tucker, Camila Shirota, Olivier Lambercy, James S. Sulzer, and Roger Gassert. Design and Characterization of an Exoskeleton for Perturbing the Knee during Gait. *IEEE Transactions on Biomedical Engineering*, 64(10):2331–2343, 2017.

[55] Max K. Shepherd and Elliott J. Rouse. Design and Validation of a Torque-Controllable Knee Exoskeleton for Sit-to-Stand Assistance. *IEEE/ASME Transactions on Mechatronics*, 22(4):1695–1704, 2017.

[56] John H Challis, Samantha L Winter, and Adam J Kuperavage. Comparison of male and female lower limb segment inertial properties. *Journal of Biomechanics*, 45(15):2690–2692, 2012.

[57] A. Pachi and Tianjian Ji. Frequency and velocity of people walking. *Structural Engineer*, 84(3):36–40, 2005.

[58] George Fulk, Miriam Ludwig, Kari Dunning, Sue Golden, Pierce Boyne, and Trent West. Estimating clinically important change in gait speed in people with stroke undergoing outpatient rehabilitation. *Journal of Neurologic Physical Therapy : JNPT*, 35:82–9, 06 2011.

[59] Christopher Akosile, Babatunde Adegoke, Anyanwu CC, Raji NO, and Orji GC. Gait quality and physical functioning of stroke survivors with and without aphasia. *Hong Kong Physiotherapy Journal*, 31, 12 2012.

[60] Elliott J. Rouse, Levi J. Hargrove, Eric J. Perreault, Michael A. Peshkin, and Todd A. Kuiken. Development of a mechatronic platform and validation of methods for estimating ankle stiffness during the stance phase of walking. *Journal of Biomechanical Engineering*, 135(8):1–8, 2013.

[61] Elliott J Rouse, Levi J Hargrove, Eric J Perreault, and Todd A Kuiken. Estimation of human ankle impedance during the stance phase of walking. *IEEE Transactions on Neural Systems and Rehabilitation Engineering*, 22(4):870–878, 2014.

[62] Ernst K Franke. Mechanical impedance of the surface of the human body. *Journal of applied physiology*, 3(10):582–590, 1951.

[63] Rolf R Coermann. The mechanical impedance of the human body in sitting and standing position at low frequencies. *Human factors*, 4(5):227–253, 1962.

[64] Brian E Lawson, Jason Mitchell, Don Truex, Amanda Shultz, Elissa Ledoux, and Michael Goldfarb. A robotic leg prosthesis: Design, control, and implementation. *IEEE Robotics & Automation Magazine*, 21(4):70–81, 2014.

[65] Max K Shepherd and Elliott J Rouse. The vspa foot: A quasi-passive ankle-foot prosthesis with continuously variable stiffness. *IEEE Transactions on Neural Systems and Rehabilitation Engineering*, 25(12):2375–2386, 2017.

[66] Amanda L Shorter, James K Richardson, Suzanne B Finucane, Varun Joshi, Keith Gordon, and Elliott J Rouse. Characterization and clinical implications of ankle impedance during walking in chronic stroke. *Scientific reports*, 11(1):16726, 2021.

[67] Robert E Kearney and Ian W Hunter. System identification of human joint dynamics. *Critical reviews in biomedical engineering*, 18(1):55–87, 1990.

[68] Hyunglae Lee, Elliott J Rouse, and Hermano Igo Krebs. Summary of human ankle mechanical impedance during walking. *IEEE journal of translational engineering in health and medicine*, 4:1–7, 2016.

[69] Amanda L Shorter and Elliott J Rouse. Mechanical impedance of the ankle during the terminal stance phase of walking. *IEEE Transactions on Neural Systems and Rehabilitation Engineering*, 26(1):135–143, 2017.

[70] Mehmet Temel, Katherine S Rudolph, and Sunil K Agrawal. Gait recovery in healthy subjects: Perturbations to the knee motion with a smart knee brace. *Advanced Robotics*, 25(15):1857–1877, 2011.

[71] Michael R Tucker, Camila Shirota, Olivier Lambercy, James S Sulzer, and Roger Gassert. Design and characterization of an exoskeleton for perturbing the knee during gait. *IEEE Transactions on Biomedical Engineering*, 64(10):2331–2343, 2017.

[72] Christopher Nesler, Gray Thomas, Nikhil Divekar, Elliott J Rouse, and Robert D Gregg. Enhancing voluntary motion with modular, backdrivable, powered hip and knee orthoses. *IEEE Robotics and Automation Letters*, 7(3):6155–6162, 2022.

[73] Zachary Bons, Gray C Thomas, Luke M Mooney, and Elliott J Rouse. A compact, two-part torsion spring architecture. In *2023 IEEE International Conference on Robotics and Automation (ICRA)*, pages 7461–7467. IEEE, 2023.

[74] David A Winter. Kinematic and kinetic patterns in human gait: variability and compensating effects. *Human movement science*, 3(1-2):51–76, 1984.

[75] M Jacquelin Perry. Gait analysis: normal and pathological function. *New Jersey: SLACK*, 2010.

[76] Yves F Nazon, Raveena M Doshi, and Elliott J Rouse. Validation of methods for estimation of knee joint mechanical impedance during locomotion using a torque-controllable knee exoskeleton. *Journal of Biomechanical Engineering*, 144(4):041005, 2022.

[77] Anindo Roy, Hermano Igo Krebs, Dustin J Williams, Christopher T Bever, Larry W Forrester, Richard M Macko, and Neville Hogan. Robot-aided neurorehabilitation: a novel robot for ankle rehabilitation. *IEEE transactions on robotics*, 25(3):569–582, 2009.

[78] Evandro M Ficanha, Guilherme A Ribeiro, and Mohammad Rastgaar. Design and evaluation of a 2-dof instrumented platform for estimation of the ankle mechanical impedance in the sagittal and frontal planes. *IEEE/ASME Transactions on Mechatronics*, 21(5):2531–2542, 2016.

[79] Robert E Kearney, Richard B Stein, and Luckshman Parameswaran. Identification of intrinsic and reflex contributions to human ankle stiffness dynamics. *IEEE transactions on Biomedical Engineering*, 44(6):493–504, 1997.

[80] Amanda L Shorter, Suzanne Finucane, and Elliott J Rouse. Ankle mechanical impedance during waling in chronic stroke: Preliminary results. In *2019 IEEE 16th International Conference on Rehabilitation Robotics (ICORR)*, pages 246–251. IEEE, 2019.

[81] Serge Pfeifer, Robert Riener, and Heike Vallery. Knee stiffness estimation in physiological gait. In *2014 36th Annual International Conference of the IEEE Engineering in Medicine and Biology Society*, pages 1607–1610. IEEE, 2014.

[82] Todd C Pataky. Generalized n-dimensional biomechanical field analysis using statistical parametric mapping. *Journal of biomechanics*, 43(10):1976–1982, 2010.

[83] David A Winter. *Biomechanics and motor control of human movement*. John wiley & sons, 2009.

[84] Elliott J Rouse, Robert D Gregg, Levi J Hargrove, and Jonathon W Sensinger. The difference between stiffness and quasi-stiffness in the context of biomechanical modeling. *IEEE Transactions on Biomedical Engineering*, 60(2):562–568, 2012.

[85] Guoping Zhao, Martin Grimmer, and Andre Seyfarth. The mechanisms and mechanical energy of human gait initiation from the lower-limb joint level perspective. *Scientific Reports*, 11(1):22473, 2021.

[86] Carl D Hoover, George D Fulk, and Kevin B Fite. Stair ascent with a powered transfemoral prosthesis under direct myoelectric control. *IEEE/ASME Transactions on Mechatronics*, 18(3):1191–1200, 2012.

[87] Levi J Hargrove, Ann M Simon, Robert Lipschutz, Suzanne B Finucane, and Todd A Kuiken. Non-weight-bearing neural control of a powered transfemoral prosthesis. *Journal of neuroengineering and rehabilitation*, 10:1–11, 2013.

[88] Nikos Karavas, Arash Ajoudani, Nikos Tsagarakis, Jody Saglia, Antonio Bicchi, and Darwin Caldwell. Tele-impedance based stiffness and motion augmentation for a knee exoskeleton device. In *2013 IEEE international conference on robotics and automation*, pages 2194–2200. IEEE, 2013.

[89] Tyler R Clites, Max K Shepherd, Kimberly A Ingraham, Leslie Wontorcik, and Elliott J Rouse. Understanding patient preference in prosthetic ankle stiffness. *Journal of neuroengineering and rehabilitation*, 18(1):1–16, 2021.

[90] Juanjuan Zhang, Pieter Fiers, Kirby A Witte, Rachel W Jackson, Katherine L Poggensee, Christopher G Atkeson, and Steven H Collins. Human-in-the-loop

optimization of exoskeleton assistance during walking. *Science*, 356(6344):1280–1284, 2017.

[91] Kimberly A Ingraham, Maegan Tucker, Aaron D Ames, Elliott J Rouse, and Max K Shepherd. Leveraging user preference in the design and evaluation of lower-limb exoskeletons and prostheses. *Current Opinion in Biomedical Engineering*, page 100487, 2023.

[92] Kimberly A Ingraham, C David Remy, and Elliott J Rouse. The role of user preference in the customized control of robotic exoskeletons. *Science robotics*, 7(64):eabj3487, 2022.

[93] Amy Blank, Allison M Okamura, and Louis L Whitcomb. Task-dependent impedance improves user performance with a virtual prosthetic arm. In *2011 IEEE International Conference on Robotics and Automation*, pages 2235–2242. IEEE, 2011.

[94] T Kevin Best, Cara Gonzalez Welker, Elliott J Rouse, and Robert D Gregg. Data-driven variable impedance control of a powered knee–ankle prosthesis for adaptive speed and incline walking. *IEEE Transactions on Robotics*, 2023.

[95] Natalie Mrachacz-Kersting and Thomas Sinkjær. Reflex and non-reflex torque responses to stretch of the human knee extensors. *Experimental brain research*, 151:72–81, 2003.

[96] John D. Brooke, William E. McIlroy, David F. Collins, and John E. Misiaszek. Mechanisms within the human spinal cord suppress fast reflexes to control the movement of the legs. *Brain Research*, 679(2):255–260, 1995.

[97] Samuel Au, Max Berniker, and Hugh Herr. Powered ankle-foot prosthesis to assist level-ground and stair-descent gaits. *Neural Networks*, 21(4):654–666, 2008.

[98] He Huang, Fan Zhang, Levi J Hargrove, Zhi Dou, Daniel R Rogers, and Kevin B Englehart. Continuous locomotion-mode identification for prosthetic legs based on neuromuscular–mechanical fusion. *IEEE Transactions on Biomedical Engineering*, 58(10):2867–2875, 2011.

[99] Cesar Ferreira, Tomás Cunha, Cristina P Santos, and Luis Paulo Reis. Torque controlled biped model through a bio-inspired controller using adaptive learning. In *2018 IEEE/RSJ International Conference on Intelligent Robots and Systems (IROS)*, pages 4369–4374. IEEE, 2018.

[100] John H Hollman, Molly K Watkins, Angela C Imhoff, Carly E Braun, Kristen A Akervik, and Debra K Ness. A comparison of variability in spatiotemporal gait parameters between treadmill and overground walking conditions. *Gait & posture*, 43:204–209, 2016.

[101] T Kevin Best, Kyle R Embry, Elliott J Rouse, and Robert D Gregg. Phase-variable control of a powered knee-ankle prosthesis over continuously varying speeds and inclines. In *2021 IEEE/RSJ International Conference on Intelligent Robots and Systems (IROS)*, pages 6182–6189. IEEE, 2021.

[102] T. Kevin Best, Cara Gonzalez Welker, Elliott J. Rouse, and Robert D. Gregg. Data-driven variable impedance control of a powered knee–ankle prosthesis for adaptive speed and incline walking. *IEEE Transactions on Robotics*, 39(3):2151–2169, 2023.

[103] Amanda L Shorter, James K Richardson, Suzanne B Finucane, Varun Joshi, Keith Gordon, and Elliott J Rouse. Characterization and clinical implications of ankle impedance during walking in chronic stroke. *Scientific Reports*, 11(1):16726, August 2021.